GENETICS

Polycomb repressive complex 1 modifies transcription of active genes

Michelle Pherson, Ziva Misulovin, Maria Gause, Kathie Mihindukulasuriya, Amanda Swain, Dale Dorsett*

Copyright © 2017 The Authors, some rights reserved; exclusive licensee American Association for the Advancement of Science. No claim to original U.S. Government Works. Distributed under a Creative Commons Attribution NonCommercial License 4.0 (CC BY-NC).

This study examines the role of Polycomb repressive complex 1 (PRC1) at active genes. The PRC1 and PRC2 complexes are crucial for epigenetic silencing during development of an organism. They are recruited to Polycomb response elements (PREs) and establish silenced domains over several kilobases. Recent studies show that PRC1 is also directly recruited to active genes by the cohesin complex. Cohesin participates broadly in control of gene transcription, but it is unknown whether cohesin-recruited PRC1 also plays a role in transcriptional control of active genes. We address this question using genome-wide RNA sequencing (RNA-seq) and chromatin immunoprecipitation sequencing (ChIP-seq). The results show that PRC1 influences transcription of active genes, and a significant fraction of its effects are likely direct. The roles of different PRC1 subunits can also vary depending on the gene. Depletion of PRC1 subunits by RNA interference alters phosphorylation of RNA polymerase II (Pol II) and occupancy by the Spt5 pausing-elongation factor at most active genes. These effects on Pol II phosphorylation and Spt5 are likely linked to changes in elongation and RNA processing detected by nascent RNA-seq, although the mechanisms remain unresolved. The experiments also reveal that PRC1 facilitates association of Spt5 with enhancers and PREs. Reduced Spt5 levels at these regulatory sequences upon PRC1 depletion coincide with changes in Pol II occupancy and phosphorylation. Our findings indicate that, in addition to its repressive roles in epigenetic gene silencing, PRC1 broadly influences transcription of active genes and may suppress transcription of nonpromoter regulatory sequences.

INTRODUCTION

Polycomb (Pc) group (PcG) protein complexes, including PRC1, PRC2, PR-DUB, and others, mediate epigenetic silencing of genes that control development throughout cell lineages (*1*–*6*). The Enhancer of zeste [E(z)] subunit of the PRC2 complex catalyzes methylation of the Lys^{27} residue of histone H3 (H3K27me3) at silenced genes, gene complexes, and their regulatory sequences, and genetic experiments in *Drosophila* show that H3K27me3 is required for silencing (*7*). The Pc subunit of the PRC1 complex binds the H3K27me3 mark (*8*), and at many genes, the Sce (sex combs extra) subunit of PRC1 ubiquitinylates the histone H2A tail (*9*). Although loss of H2A ubiquitinylation is lethal, it is not required for gene silencing (*10*).

Recent studies have revealed that PRC1 subunits are also present at many active gene promoters that lack H3K27me3 (*11*–*14*). PRC1 directly interacts with the cohesin protein complex that is present at many active promoters (*14*, *15*). Cohesin not only mediates sister chromatid cohesion to ensure proper chromosome segregation but also functions in multiple gene control mechanisms, including facilitating long-range enhancer-promoter communication (*16*). Genomic chromatin immunoprecipitation (ChIP) experiments show that depletion of cohesin decreases PRC1 occupancy of active promoters and increases PRC1 levels at silenced genes (*14*). One interpretation of this finding is that cohesin sequesters PRC1 at active promoters, limiting the availability for binding to silenced genes (*17*). Consistent with this idea, cohesin mutations dominantly suppress developmental defects caused by PRC1 haploinsufficiency and vice versa (*14*, *18*, *19*). Stabilization of cohesin binding by partial inactivation of the Wapl protein that removes cohesin from chromosomes causes developmental transformations similar to those caused by PRC1 insufficiency, further supporting the idea that cohesin controls PRC1 availability (*20*).

Edward A. Doisy Department of Biochemistry and Molecular Biology, Saint Louis University School of Medicine, Saint Louis, MO 63104, USA.
*Corresponding author. Email: dorsettd@slu.edu

The presence of PRC1 at active genes suggests that it has a role in regulating their transcription. Cohesin and the Nipped-B protein that loads cohesin onto chromosomes preferentially bind genes at which RNA polymerase II (Pol II) initiates transcription but pauses just downstream of the transcription start site (*21*, *22*). Nipped-B and cohesin have little effect on Pol II recruitment but modulate transition of paused Pol II into elongation. They facilitate transition at many genes and inhibit elongation at many others. Previous studies suggest that the PRC1 recruited by cohesin may participate in the mechanisms by which cohesin modulates the activity of Pol II at active genes (*14*).

Here, we examine how PRC1 affects transcription of active genes using RNA sequencing (RNA-seq), 3′ nascent RNA-seq (3′ NT-seq), and ChIP sequencing (ChIP-seq) for various forms of RNA polymerase (Pol II) and the Spt5 pausing-elongation factor. The results show that RNA interference (RNAi)–mediated depletion of PRC1 subunits in cultured *Drosophila* cells alters transcription of several active genes and that the affected genes are enriched for those that bind higher levels of PRC1. PRC1 depletion alters Pol II phosphorylation and Spt5 levels at most active genes and transcriptional enhancers. These effects coincide with changes in nascent RNA density that indicate altered transcriptional elongation and RNA processing. These findings demonstrate that PRC1 acts broadly beyond its role at epigenetically silenced genes to control transcription.

RESULTS

Depletion of PRC1 subunits alters transcription of many active genes

We tested the idea that PRC1 influences the transcription of active genes by using RNAi to deplete PRC1 subunits in ML-DmBG3-c2 (BG3) cells derived from larval central nervous system and by measuring transcript accumulation and transcription by RNA-seq. As our laboratory previously reported, depletion of PRC1 subunits in BG3 cells alters cell morphology and causes them to stop dividing after 6 to 7 days of depletion

(*14*); therefore, we isolated RNA after 4 to 5 days of depletion. Western blots show that Ph (polyhomeotic) depletion is incomplete, although greater than 50% in all experiments (see below). Sce depletion moderately reduces total Ph levels and strongly reduces Pc and ubiquitinylated histone H2A (H2Aub). These effects of Sce depletion on other PRC1 subunits and H2Aub are similar to those seen in vivo with *Sce* mutants (*10*). Ph depletion, in contrast, reduces Pc and H2Aub to a lesser degree than does Sce depletion.

We used ribosomal depletion of total RNA to measure transcript accumulation and 3′ NT-seq to measure transcription. 3′ NT-seq is adapted from the method used by Weber *et al.* (*23*) to measure active 3′ elongating RNA ends and is similar to a method described by Churchman and Weissman (*24*). The RNA-seq and 3′ NT-seq values for all expressed genes are in table S1. In controls, the density (nucleotide coverage per gene base pair) of 3′ NT-seq correlates well with the total RNA-seq density (nucleotide coverage per transcript nucleotide) with a Pearson correlation coefficient of 0.75, indicating that transcription is a key driver of transcript accumulation.

As expected, depletion of the Ph subunit of PRC1 increases the accumulation of RNAs from many Pc-silenced genes and increases their transcription as measured by 3′ NT-seq (Fig. 1A and table S1). Many genes that are not Pc-silenced also show increases in transcription and RNA accumulation, and a smaller number show decreases. There is a significant correlation between the fold changes in 3′ NT-seq and transcript accumulation ($r = 0.61$; Fig. 1B), and many of the genes that show significant changes in RNA accumulation (Fig. 1B, left, red dots) also show significant changes in transcription (Fig. 1B, right, orange dots). Nonetheless, a small number of genes show increased RNA accumulation even with decreased transcription. Many of these opposite changes in transcription and RNA accumulation are statistically significant ($q \leq 0.05$). There

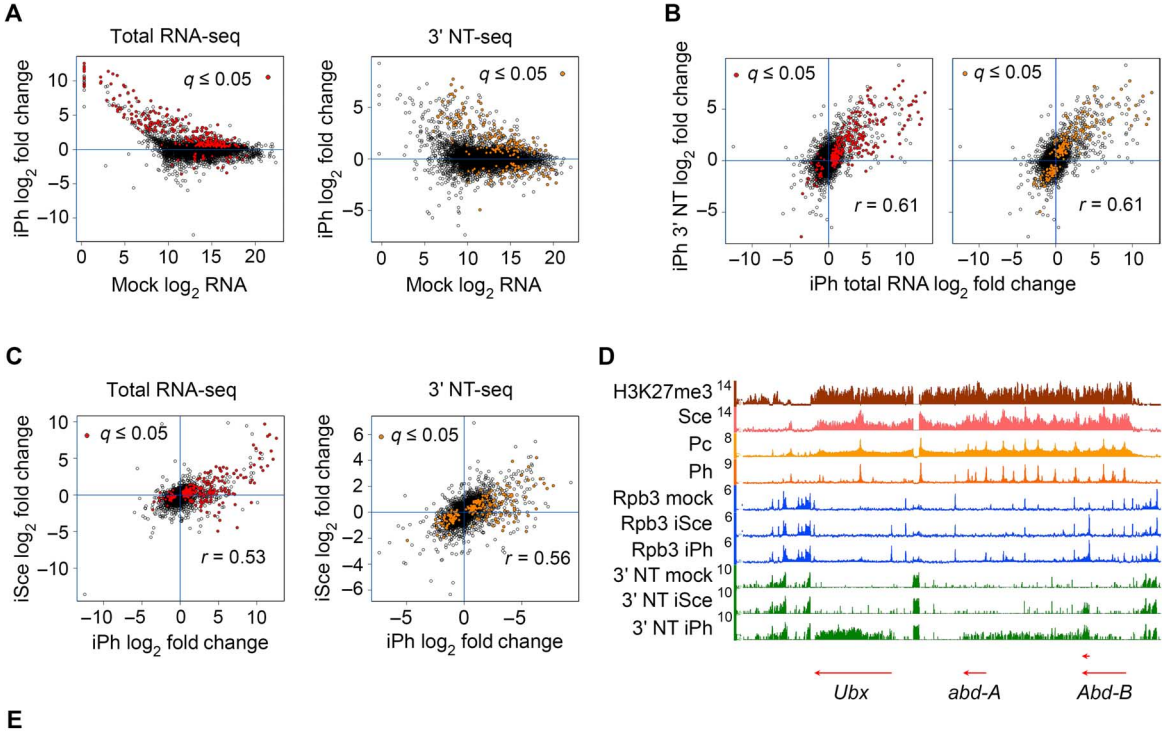

E

	Total	PcG Domain	NOT PcG Domain		High Ph	Low Ph	
Expressed genes	7561	73	7488	Fisher's exact test	3768	3793	Fisher's exact test
iPh UP total	267	49	218	6.20E–41	185	82	1.10E–10
iPh DOWN total	29	0	29	7.60E–01	14	15	1.50E–01
iPh UP 3′ nascent	133	21	112	3.10E–18	86	47	2.10E–04
iPh DOWN 3′ nascent	61	0	61	5.50E–01	38	23	1.60E–02

Fig. 1. PRC1 modifies transcription of active genes in BG3 cells. (**A**) Effects of Ph depletion (iPh) on transcript accumulation (total RNA-seq) and transcription (3′ NT-seq). The left dot plot shows the $\log_2$ fold change in RNA levels from expressed genes upon Ph depletion versus the $\log_2$ RNA level in the mock-treated control cells using total RNA-seq. Red points are genes in which the change in total RNA levels caused by Ph depletion is significant at a false discovery rate of ≤5% ($q \leq 0.05$). The right dot plot shows the same by 3′ NT-seq. Orange indicates where the change is statistically significant ($q \leq 0.05$). (**B**) Both dot plots show the fold change in RNA accumulation (total RNA) versus that in transcription (3′ NT-seq) upon Ph depletion (iPh). The two graphs are identical except that the left shows which changes are significant by total RNA-seq (red dots) and the right shows those significant by 3′ NT-seq (orange dots). (**C**) The left dot plot shows the fold change in RNA upon Ph depletion (iPh) versus the fold change upon Sce depletion (iSce) by total RNA-seq. Red dots show the changes that are statistically significant ($q \leq 0.05$) upon Ph depletion. The right dot plot shows the same by 3′ NT-seq. Orange dots show changes that are statistically significant ($q \leq 0.05$) upon Ph depletion. (**D**) Genome browser view of the bithorax complex shows occupancy by H3K27me3 [modENCODE ChIP-chip; Gene Expression Omnibus (GEO) GSE20780] and Sce (modENCODE ChIP-chip; GEO GSE20817) in BG3 cells; Pc, Ph, and Rpb3 ChIP-seq enrichment in control cells (this study); Rpb3 ChIP-seq in cells depleted for Sce (Rpb3 iSce) and Ph (Rpb3 iPh); and 3′ NT-seq data for mock control cells and cells depleted for Sce or Ph. The ChIP-chip enrichment scale is MAT score, and the ChIP-seq data scale is $\log_2$ enrichment. The RNA-seq data scales are $\log_2$ nucleotide coverage (density). (**E**) Enrichment of genes that change in transcript accumulation or transcription upon Ph depletion for those that have high levels of Ph. Increases (UP) and decreases (DOWN) in RNA levels were defined as those with $q \leq 0.05$. *P* values were calculated using Fisher's exact test.

are also genes that show increased transcription but lower RNA accumulation. This indicates that RNA processing and stability are altered for some genes.

The significant effects of Ph depletion (iPh) on RNA levels and transcription are more numerous and generally stronger than those caused by depletion of the Sce PRC1 subunit (iSce; Fig. 1C and table S1). The Pearson correlation between fold changes in RNA accumulation with Ph and Sce depletion is 0.53, and the correlation between fold changes in transcription (3′ NT-seq) is 0.56. Strikingly, several genes that show significant increases in transcription and RNA accumulation with Ph depletion show decreases with Sce depletion (Fig. 1C). This indicates that the roles of individual PRC1 subunits can vary depending on the gene.

We also conducted total RNA-seq after Pc depletion, finding that the effects correlate well with both Sce and Ph depletion (table S1 and fig. S1). Pc depletion has overall stronger effects than Sce depletion, resulting in more statistically significant changes in RNA levels. The Pearson correlation between fold changes in RNA levels with Pc and Sce depletion is 0.70 and 0.66 between Pc and Ph depletion. Thus, although the transcriptional effects of Sce depletion are generally weaker, they correlate well with the effects of depleting other PRC1 subunits.

Figure 1D is a genome browser view of the bithorax HOX gene complex that illustrates some of the differences in the effects of Sce and Ph depletion. As illustrated by the 3′ NT-seq tracks, Sce depletion increases the transcription of a shorter *Abd-B* transcription unit but has little effect on other genes in the complex. In contrast, Ph depletion increases the transcription of multiple *Abd-B* transcription units and the *Ubx* and *abd-A* genes. Ph depletion also increases the transcription of the intergenic region between *Abd-B* and *abd-A*. ChIP-seq for the Rpb3 Pol II subunit (described below) shows substantial increases in Pol II levels at the *Abd-B*, *abd-A*, and *Ubx* promoters with Ph depletion, and at the *Abd-B* and *Ubx* promoters with Sce depletion.

Statistical analysis supports the idea that many of the effects of PRC1 depletion on active gene transcription are direct. Genes were classified as binding high or low Ph levels, or as PcG domain genes as described in Materials and Methods. Figure 1E shows that using Fisher's exact test, the active genes that increase in transcription and produce higher steady-state transcript levels upon Ph depletion ($q \leq 0.05$) are enriched for those occupied by higher levels of Ph. Genes that produce less total RNA are not enriched for those with high Ph levels, although the 61 genes that show significant decreases in transcription by 3′ NT-seq are enriched for those with high Ph levels ($P = 1.6 \times 10^{-2}$). Although this analysis argues that PRC1 directly affects the transcription of many active genes, variability in effects from gene to gene, coupled with the likelihood of indirect effects, prevents drawing conclusions about direct effects at any individual gene.

Gene ontology analysis indicates that the genes that significantly increase ($q \leq 0.05$) in RNA accumulation upon Ph depletion are significantly enriched for those encoding transcription factors and genes involved in imaginal disc development and organ morphogenesis (table S1). There were insufficient genes with reduced mRNA accumulation for ontology analysis, but the genes that decrease in transcription (3′ NT-seq) upon Ph depletion are enriched for those involved in axonogenesis and neuron development. This suggests that PRC1 depletion reprograms BG3 cells from a neural to an imaginal disc or organ differentiation pathway.

Depletion of PRC1 subunits alters levels of other PRC1 subunits and their association with genes and gene regulatory sequences

Interpretation of how Ph and Sce depletion differentially alter gene expression needs to account for how their depletion alters the levels of other PRC1 subunits and their occupancy of active genes and regulatory sequences. Ph ChIP-seq was performed in Pc- and Sce-depleted cells, and Pc ChIP-seq was performed in cells depleted for Ph and Sce. Multiple biological replicates were performed for each ChIP-seq. The ChIP-seq data were used for metagene analysis (Fig. 2A) and to quantify the enrichment of PRC1 subunits at active gene promoters, transcriptional enhancers, and Pc response elements (PREs) (Fig. 2B). Western blots for Ph, Pc, and H2Aub after Sce, Ph, and Pc depletion are shown in Fig. 2C, and the results of all analyses are summarized in Fig. 2D. Dot plots showing the effects on PRC1 subunit levels at all individual gene regulatory sequences are shown in figs. S2 and S3, and statistical analysis of the metagene and regulatory sequence data is presented in table S2. In general, although Sce depletion has smaller effects than Ph depletion on transcription (Fig. 1), it has stronger effects on the levels of other PRC1 subunits and their binding to genes and regulatory sequences. Thus, the stronger effects of Ph depletion on transcription seen above do not reflect changes in the levels or binding of other PRC1 subunits.

Genes were classified into different groups for the metagene analysis, as described in Materials and Methods. The largest group of active genes (Ph+ H3K27me3−) has high levels of Ph and little or no H3K27me3. The second largest group (Ph− H3K27me3−) has low Ph and little H3K27me3. A small number of active genes (Ph+ H3K27me3+) have high levels of both Ph and H3K27me3. PcG domain genes have very high levels of Ph and, in addition, very high H3K27me3 over the entire length of the gene. Most of these, such as those in the bithorax complex (Fig. 1B), are silenced. Active promoters (7389), extragenic enhancers (523), and PREs (195) were defined using deoxyribonuclease I (DNase I) hypersensitivity and histone modification data, as previously described (*22*, *25*).

In the metagene plots, Ph and Pc enrichments peak just upstream of the transcription start site, with the highest mean enrichment at PcG domain genes, followed by Ph+ H3K27me3+ active genes and then Ph+ H3K27me3− genes (Fig. 2A). Ph− H3K27me3− genes also show a modest peak of Ph enrichment and, surprisingly, a similar mean enrichment for Pc as Ph+ H3K27me3− genes. Thus, the levels of Pc and Ph at active promoters, similar to regions between PREs in PcG domains (Fig. 1D), are not strictly stoichiometric. Ph and Pc enrichment is substantially higher at PREs than at active promoters and enhancers, which show similar levels (Fig. 2B).

To summarize the findings (Fig. 2D), reduction of any PRC1 subunit significantly reduces the levels of the others at PREs (Fig. 2B, figs. S2 and S3, and table S2) at silenced PcG domain genes and at Ph+ H3K27me3+ active genes (Fig. 2A and table S2). In contrast, Sce and Ph depletion increases the levels of Pc at active genes lacking H3K27me3 (Fig. 2A and table S2) and active promoters while decreasing Pc at active enhancers (Fig. 2B, fig. S3, and table S2). Sce and Pc depletions have opposite effects on Ph levels at active genes lacking H3K27me3 (Fig. 2A and table S2), promoters, and enhancers (Fig. 2B, fig. S2, and table S2). Sce depletion decreases Ph levels at these locations, whereas Pc depletion increases them. These effects are taken into account in the interpretation of the experiments described below that explore how PRC1 subunits alter gene transcription. These results indicate that, in contrast to PREs, Ph and Pc can largely associate with active genes and enhancers independently of each other.

PRC1 modifies RNA polymerase levels and transcription across active genes

To examine how PRC1 might influence transcription of active genes, we used ChIP-seq with Rpb3 antibody to quantify how PRC1 subunit depletion alters Pol II occupancy at active genes. We also examined how PRC1

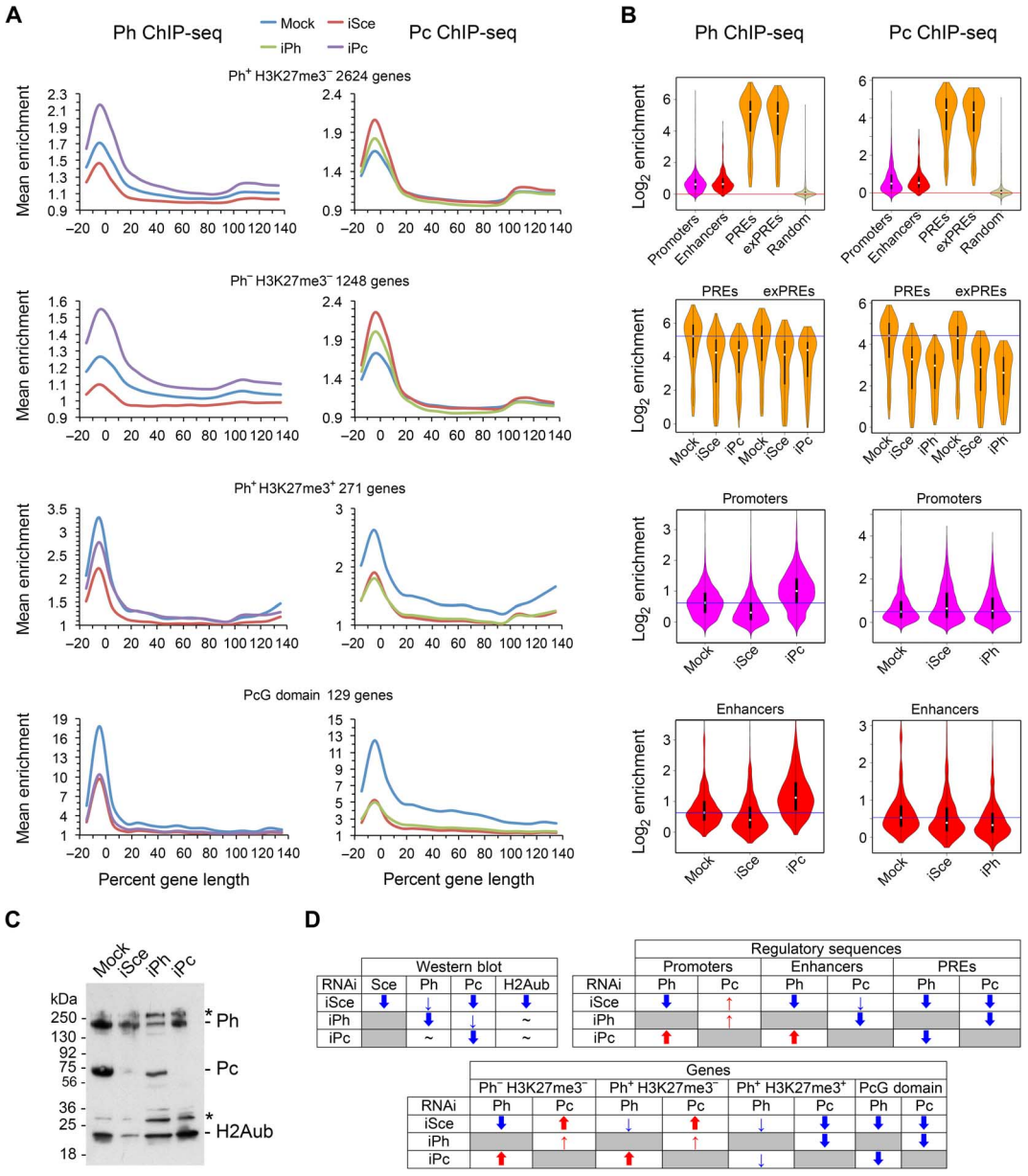

Fig. 2. PRC1 subunit depletion alters the binding of other subunits to active genes, silenced genes, and regulatory sequences in BG3 cells. (**A**) Metagene analysis of Ph and Pc ChIP-seq enrichment for four gene categories, using 16 bins from −20 to +140% of annotated gene length. Ph ChIP-seq was conducted in mock control cells (blue line), cells depleted for Sce (iSce; red line), and cells depleted for Pc (iPc; purple line). Pc ChIP-seq was conducted for mock control cells (blue line), cells depleted for Sce (red line), and cells depleted for Ph (iPh; green line). Statistical tests of the differences in enrichment between the mock control and PRC1 subunit–depleted cells are in table S2. (**B**) Effects of PRC1 subunit depletion on the binding of other PRC1 subunits to active promoters (promoters, 7389), extragenic enhancers (enhancers, 523), PREs (195), and extragenic PREs positioned outside of regions that become transcribed upon Ph or Sce depletion (exPREs; 90). The left top panel shows the violin plot distributions of Ph enrichment at active promoters, extragenic enhancers, PREs, extragenic PREs (exPREs), and 6892 random 500–base pair (bp) regions as a control. The red line indicates no enrichment (log_2 enrichment = 0). The top right panel shows the same for Pc. The left panel in the second row shows the Ph enrichment at PREs and extragenic PREs in mock control cells and cells depleted for Sce (iSce) and Pc (iPc). The blue line indicates the median enrichment level in mock control cells. The right panel in the second row shows the Pc enrichment at PREs and extragenic PREs in mock control cells and cells depleted for Sce and Ph. The left panel in the third row shows the Ph enrichment at active promoters in mock control, Sce-depleted, and Pc-depleted cells. The right panel in the third row shows the enrichment for Pc at active promoters in mock, Sce-depleted, and Ph-depleted cells. The left panel in the fourth row shows the Ph occupancy of extragenic enhancers in mock control, Sce-depleted, and Pc-depleted cells, and the right panel shows Pc enrichment at enhancers in mock, Sce-depleted, and Ph-depleted cells. All effects on Ph binding to regulatory sequences are also illustrated by dot plots in fig. S2, and all effects on Pc binding are shown in fig. S3. (**C**) Example Western blot showing levels of Ph, Pc, and H2Aub in whole-cell extracts of mock control, Sce-depleted (iSce), Ph-depleted (iPh), and Pc-depleted (iPc) cells. The top asterisk (*) indicates Ph protein produced by the *ph-p* gene, and the lower asterisk indicates di-ubiquitinylated H2A ($H2Aub_2$) (*10*). Ph and Pc depletions often enhance the levels of these variants, but the degree of enhancement varies between experiments. (**D**) Table summarizing the effects of depleting Sce, Ph, and Pc on Sce, Ph, Pc, and H2Aub levels by Western blot and ChIP-seq at various regulatory sequences and genes. Thick blue arrows indicate large decreases, thin blue arrows indicate weak to moderate decreases, thick red arrows indicate large increases, and thin red arrows indicate weak to moderate increases. Tildes (~) indicate no obvious change, and gray boxes indicate that the levels were not measured.

subunit depletion alters 3′ NT-seq density across genes, as a more direct measure of transcription. As detailed below, we find that Pol II levels are only slightly altered on most active genes upon PRC1 depletion, and that there are effects on transcription near the ends of genes consistent with changes in transcription levels, elongation, and/or RNA processing.

As expected, Rpb3 enrichment peaks just downstream of transcription start sites, where promoter-proximal pausing occurs, and remains relatively level across gene bodies with a small peak past the ends of genes, where transcription termination occurs (Fig. 3A). The 3′ NT-seq density across gene bodies is low at promoters because library construction does not capture 5′ capped RNA fragments. Transcription density is mostly level across gene bodies and declines sharply at the ends where transcription passes polyadenylation sites (Fig. 3A). The 3′ NT-seq procedure degrades nascent RNAs cleaved for polyadenylation, so

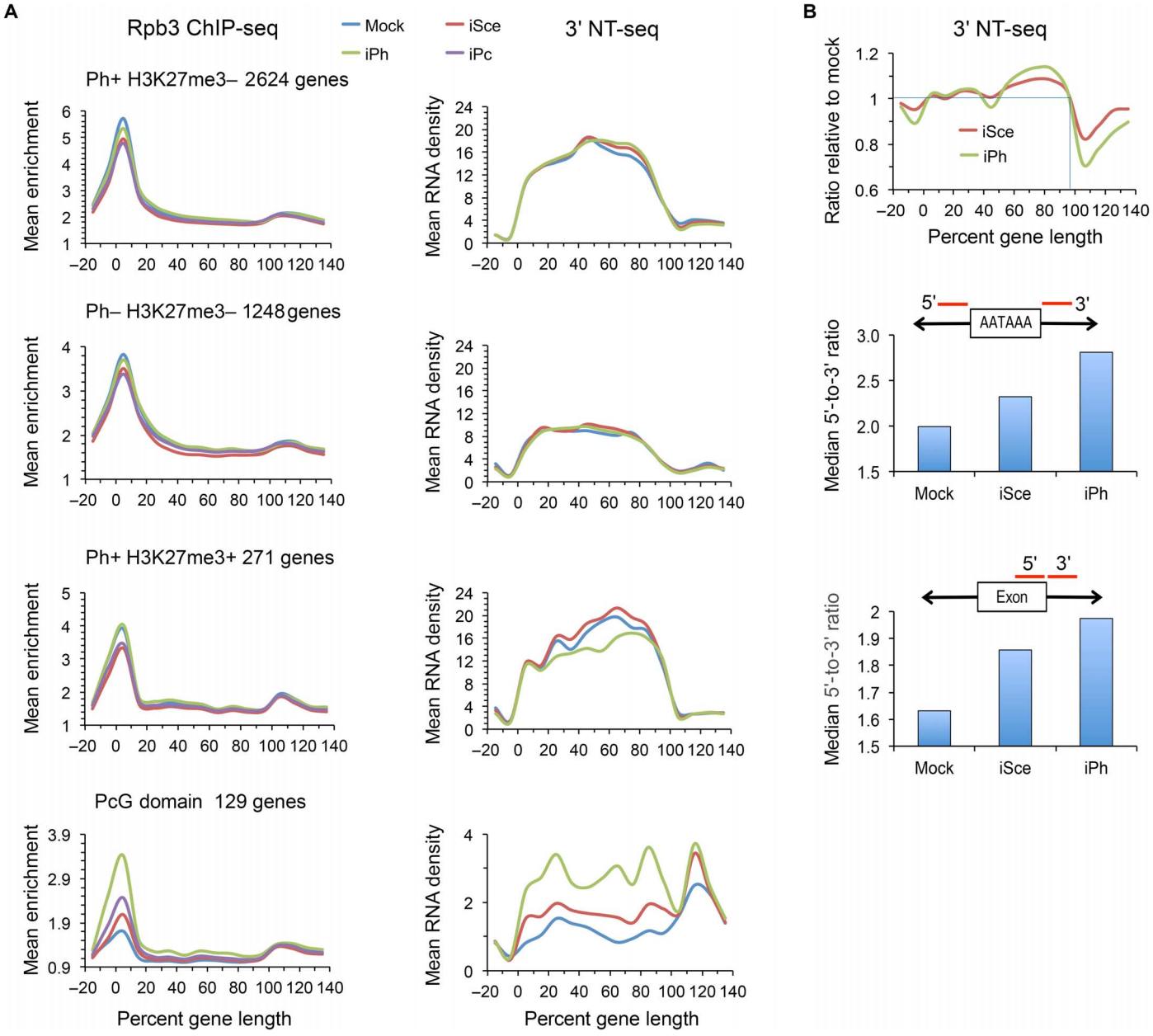

Fig. 3. PRC1 subunits alter transcription (3′ NT-seq) and Pol II (Rpb3) occupancy of active genes. (**A**) Metagene analysis of Rpb3 ChIP-seq (left) and 3′ NT-seq (right) for three active gene categories for mock control (blue lines), Sce-depleted (iSce; red lines), Ph-depleted (iPh; green lines), and Pc-depleted (iPc; purple lines) cells. Statistical tests of the enrichment differences between mock control and PRC1 subunit–depleted cells are in table S2. (**B**) Top: Ratio of 3′ NT-seq metagene density in Sce- and Ph-depleted cells to the 3′ NT-seq density in mock control cells for Ph+ H3K27me3– genes [upper right panel in (A)]. The horizontal and vertical blue lines intersect at the average position of the poly(A) sites, determined by performing a metagene analysis with total RNA-seq data (not depicted). Middle: Median ratio of the 3′ NT-seq density in the 500 nucleotides (nt) upstream of AATAAA sequences to the density in the 500 nt downstream of the AATAAA sequences for all active genes in mock control, Sce-depleted, and Ph-depleted cells. Bottom: Ratio of the 3′ NT-seq data in the last 500 nt of exons to the first 500 nt of the following intron in mock control, Sce-depleted, and Ph-depleted cells.

transcription downstream of polyadenylation [poly(A)] sites is not fully captured. Figure 4A shows the example of the *headcase* gene with typical Rpb3 ChIP-seq and 3′ NT-seq profiles.

There is a significant difference in the mean levels of Rpb3 and transcription between the active genes with high Ph levels (Ph+ H3K27me3−) and low Ph levels (Ph− H3K27me3−) (Fig. 3A). The genes with high Ph show about 50% greater Rpb3 enrichment at the promoter and some twofold higher levels of 3′ NT-seq density in the gene bodies. The difference in Rpb3 levels at the promoters is significant ($P = 4.1 \times 10^{-16}$, unpaired Wilcoxon test). The Pearson correlation between the mean enrichment of Ph and Rpb3 across all 7389 active promoters is 0.51, supporting the idea that genes with more Pol II generally

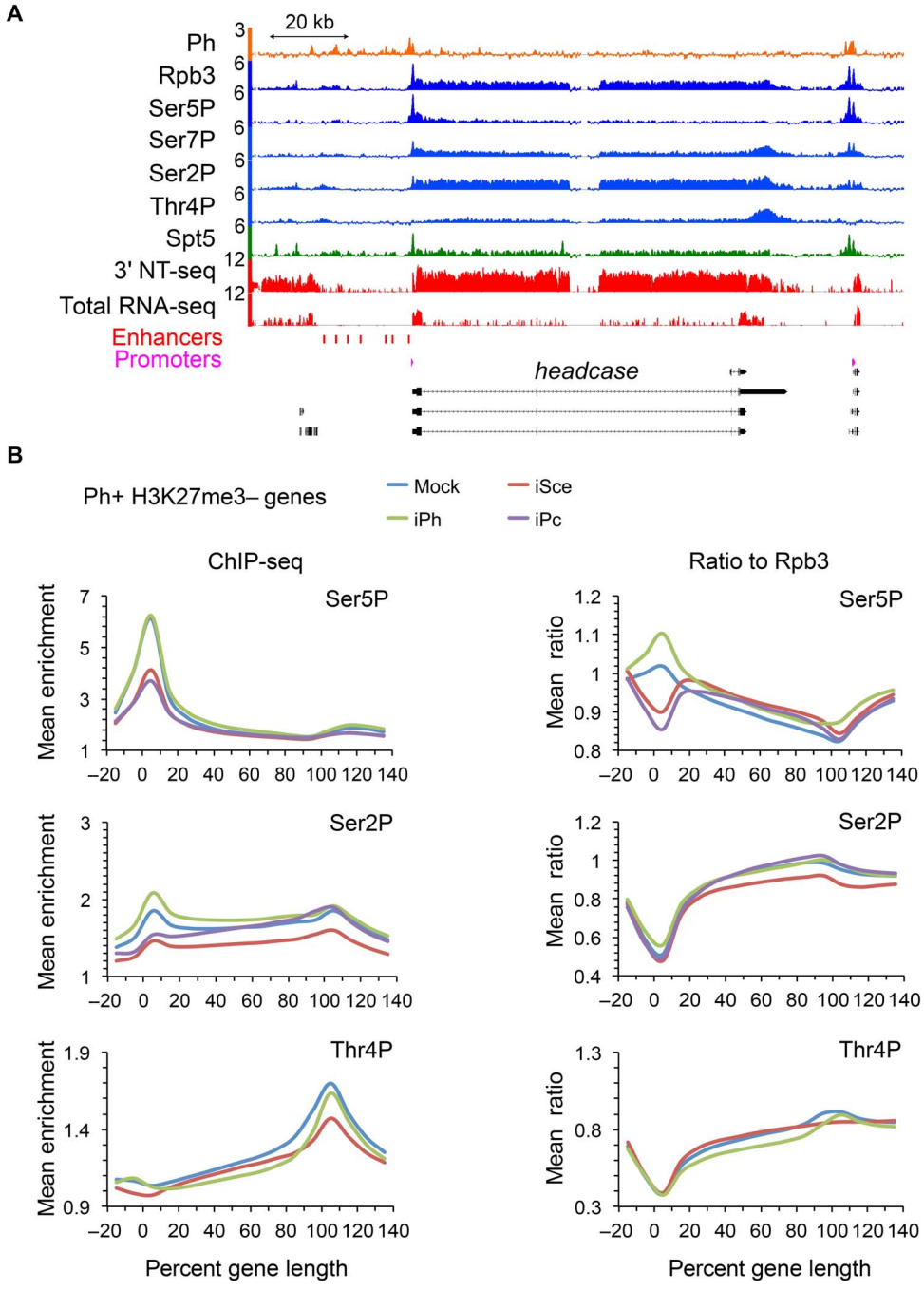

Fig. 4. PRC1 subunits alter phosphorylation of the Rpb1 CTD heptad repeats. (**A**) Genome browser view of the *headcase* gene (transcribed from left to right) as an example showing a typical ChIP-seq $\log_2$ enrichment pattern for the Ph, Rpb3, Ser5P, Ser7P, Ser2P, Thr4P, and Spt5 antibodies. The $\log_2$ densities for 3′ NT-seq and total RNA-seq are shown for comparison. (**B**) Metagene analysis of the Ser5P, Ser2P, and Thr4P enrichment for Ph+ H3K27me3− genes in mock control (blue lines), Sce-depleted (iSce; red lines), Ph-depleted (iPh; green lines), and Pc-depleted (iPc; purple) cells. Left: Mean enrichment for each modification. Right: Ratio of each modification relative to Rpb3 (see Fig. 3). Metagene patterns at other gene classes and Ser7P data are shown in fig. S4. Wilcoxon signed-rank test *P* values of the differences in peak enrichment between the mock control and PRC1 subunit–depleted cells are in table S2.

also have higher Ph levels. Unexpectedly, Ph+ H3K27me3+ genes have a similar mean enrichment of promoter Rpb3 as Ph− H3K27me3− genes but show a higher transcription level similar to that of Ph+ H3K27me3− genes (Fig. 3A). This suggests that Ph+ H3K27me3+ genes have less promoter-proximal transcriptional pausing than the other gene classes.

As expected, Sce (iSce; red), Ph (iPh; green), or Pc (iPc; purple) depletion significantly increases Rpb3 at promoters of the PcG domain genes, which correlates with their increased transcription (Fig. 3A and table S2). The Rpb3 increases with Ph depletion are larger than those with Sce depletion, consistent with the greater increases in transcription observed by RNA-seq (Fig. 1).

PRC1 subunit depletion modestly alters Rpb3 association with the promoters of active genes. For most genes, which include the Ph+ H3K27me3− and Ph− H3K27me3− categories, there are moderate decreases in Rpb3 occupancy at promoters upon Sce or Pc depletion and only slight decreases with Ph depletion (Fig. 3A). The mean changes are noticeably greater at genes with higher Ph levels (Ph+ H3K27me3−) than at those with lower Ph levels (Ph− H3K27me3−). The decreases are statistically significant at all gene classes with Sce and Pc depletion but are not significant with Ph depletion at the Ph− H2K27me3^{-} or Ph+ H3K27me3+ genes (table S2). Thus, PRC1 subunit depletion modestly but measurably decreases Pol II occupancy of most active genes. We did not quantify differences in Rpb3 levels across gene bodies because the occupancy is substantially lower than at promoters.

At first glance, the modest decreases in total promoter Pol II levels upon PRC1 subunit depletion are discordant with the findings that Ph depletion causes more statistically significant increases than decreases in RNA production from active genes and that increases in RNA production are more likely to be direct effects of Ph depletion (Fig. 1). A decrease in pausing with more Pol II entering into elongation might explain the reduced levels of Pol II levels at the promoters and increased RNA production. However, Ph depletion has a more modest effect than Sce depletion on promoter Pol II levels but a stronger effect on RNA accumulation. Thus, the changes in promoter Pol II levels do not fully account for the observed effects on transcription and RNA accumulation.

The density of 3′ nascent RNA across gene bodies measures transcription more directly than does Rpb3 ChIP-seq and is more sensitive. Transcription across approximately the first half of most active genes is not measurably altered by Sce or Ph depletion (Fig. 3A). However, there is a quantifiable increase in mean 3′ NT-seq density in the second half of the Ph+ H3K27me3− genes. This is more easily visualized by examining the ratio of the 3′ NT-seq density in the Sce and Ph depletion samples to the density in the mock control (Fig. 3B). There is a mean 5 to 10% increase relative to the control in the second half of the gene bodies, coinciding with a 20 to 30% decrease past gene ends. The transition from an increase to a decrease occurs at the average position of poly(A) sites (Fig. 3B). The increased transcription density in the second half of genes and the lower density past the gene ends upon Sce or Ph depletion suggest that there may be changes in transcription elongation, transcription termination, or RNA processing.

To more closely examine potential effects on termination, we generated a list of potential AATAAA poly(A) signals, with the consensus sequence in the proper strand located in exons in the latter third of gene bodies, and calculated the upstream-to-downstream ratio of the 3′ NT-seq transcription density for each of these potential poly(A) signals. At a functional poly(A) signal, we expect the upstream transcription density to be higher because most downstream nascent RNAs are lost during library preparation. The median upstream-to-downstream ratio for the potential poly(A) signals is approximately 2 in control cells and increases to nearly 2.3 upon Sce depletion and 2.8 upon Ph depletion (Fig. 3B). One possible explanation for this ratio increase is that less efficient RNA processing after PRC1 depletion could cause Pol II to spend more time at the poly(A) sites. An alternative is that increased transcription creates a termination and/or 3′ end processing bottleneck. This latter idea is more consistent with the observation that PRC1 subunit depletion generally increases transcription (Fig. 1).

Genes are typically more exon-rich in their second half than in their first half. Thus, a potential reason for increased 3′ NT-seq density in the second half of active genes upon PRC1 depletion is that polymerase slows in exons. Jonkers *et al.* (*26*) reported that elongating Pol II slows in exons, positing that this is associated with splicing. We thus expect to find a higher 3′ NT-seq density in exons relative to the downstream intron sequences. Using exons of 500 nt or larger, we find that the median 3′ NT-seq density is more than 1.6-fold higher in exons than in the downstream intron sequences in control cells, supporting the idea that transcription slows in exons (Fig. 3B). The median ratio increases to more than 1.8 with Sce depletion and to nearly 2 upon Ph depletion. This is consistent with the idea that PRC1 depletion slows Pol II elongation through exons. This may reflect subtle reductions in RNA splicing efficiency, or alternatively, more transcription could increase accumulation of Pol II in exons by increasing overall traffic. The data do not distinguish between these possibilities, but an increase in transcription is more consistent with the finding that Ph depletion causes more significant RNA increases than decreases (Fig. 1).

PRC1 globally modifies RNA polymerase phosphorylation

We tested the idea that PRC1 influences phosphorylation of Pol II because phosphorylation of the Rpb1 subunit C-terminal domain (CTD) supports binding of elongation and RNA processing factors and provides markers for transcription initiation and elongation (*27*, *28*). The Rpb1 CTD consists of multiple heptad repeats of a YSPTSPS consensus sequence. Although the exact roles of each modification are not fully understood, phosphorylation of Ser^{5} (Ser5P) in the heptad repeat by transcription factor IIH (TFIIH) complex coincides with transcription initiation, and phosphorylation of Ser^{2} (Ser2P) coincides with the release from pausing into active elongation. We used ChIP-seq with antibodies specific for different phosphorylated residues and metagene analysis to test how PRC1 depletion alters the Pol II phosphorylation state. The antibody specificities were demonstrated by the manufacturer with modified heptad repeat peptides (Cell Signaling Technology). All are rabbit monoclonal antibodies and thus give reproducible results from lot to lot. As described below, we find that Sce and Pc depletion generally decreases Pol II phosphorylation at active genes and that Ph depletion increases phosphorylation.

The phosphorylated Pol II–specific antibodies give the expected ChIP-seq patterns. Figure 4A shows these patterns at the *headcase* gene. As described above, Rpb3 enrichment measures total Pol II and displays a peak of paused Pol II just downstream of the transcription start site, remains level across the gene body, and peaks again past the end of the gene. Ser5P, which occurs upon initiation, peaks just downstream of the transcription start site and trails off into the gene body. Ser^{7} phosphorylated Pol II (Ser7P) peaks just downstream of the transcription start site, remains at low levels across the gene body, and peaks again just past the end of the gene. Ser2P, associated with elongation, displays level enrichment across the entire gene body, with small peaks near the transcription start site and at the end of the gene. For most active genes, Thr^{4} phosphorylated Pol II (Thr4P) potentially associated with transcription

termination (*29*) displays low enrichment across the gene body and peaks just past the end of the gene, as shown by the *headcase* gene example (Fig. 4A). However, a few active genes, such as *cut*, also display Thr4P peaks near the transcription start sites. It is important to note that these antibodies are specific to individual phosphorylated residues within heptad repeats and that most are nonreactive with heptads containing multiple phosphorylated residues. For instance, as reported by the manufacturer (Cell Signaling Technology), the Ser5P antibody does not react with heptad repeats that have both Ser2P and Ser5P residues. Thus, low Ser5P enrichment throughout a gene body does not necessarily indicate low Ser5P but could also indicate masking by additional modifications.

In general, depletions of Sce and Pc have similar effects on Pol II phosphorylation at active genes, and these differ from those caused by Ph depletion. As described above, Sce and Pc depletions have opposite effects on Ph levels at active genes and promoters (Fig. 2), indicating that the observed effects on Pol II phosphorylation described below reflect the loss of Sce or Pc and not their effects on Ph. Sce and Pc depletions substantially decrease Ser5P just downstream of transcription start sites across all active gene types, and all decreases are statistically significant (Fig. 4B, fig. S4, and table S2). Sce depletion does not significantly alter Ser5P levels at PcG domain genes, and Pc depletion causes a significant increase (table S2). The ratio of Ser5P to Rpb3 also decreases at active promoters, indicating that the fraction of Pol II molecules and/or the number of phosphorylated heptad repeats decrease (Fig. 4B). The global trend of reduced Ser5P holds true for most of the 7389 active promoters, as revealed by violin plots in Fig. 5 and dot plots in fig. S5. A decrease in Ser5P could indicate that transcription initiation is reduced. However, Rpb3 is still positioned downstream of the transcription start site (Fig. 3A), indicating that most Pol II has initiated transcription and is paused. We thus favor the idea that the decrease in Ser5P reflects primarily a decrease in the fraction of heptad repeats that are phosphorylated, rather than a decrease in the number of phosphorylated Rpb1 molecules.

Sce or Pc depletion slightly increases the Ser5P-to-Rpb3 ratio in most active gene bodies, which is opposite to the effect at promoters (Fig. 4B and fig. S4). Because phosphorylation at other residues in the heptad repeat can block recognition by the Ser5P antibodies, this increase could reflect either a higher Ser5P level or reduced phosphorylation of other residues. The Ser5P modification occurs upon transcription initiation before phosphorylation of other heptad repeat residues. Thus, we might anticipate reductions in additional downstream Pol II modifications upon Sce depletion. Ser2P is significantly reduced at the promoters (Figs. 4B and 5, figs. S4 and S5, and table S2) and across the entire body (Fig. 4B and fig. S4) of all active gene categories upon Sce depletion. The Ser2P-to-Rpb3 ratio is modestly decreased by Sce depletion at active promoters (Fig. 5) and throughout active gene bodies (Fig. 4B). Pc depletion causes a similar reduction in Ser2P at gene promoters (Figs. 4B and 5, figs. S4 and S5, and table S2), but Ser2P increases along the gene body to near-normal levels by the end (Fig. 4B). Thus, although Sce and Pc have very similar effects on Ser^5 and Ser^2 phosphorylation at promoters, they differ in their effects on Ser^2 phosphorylation in gene bodies. Sce depletion also reduces mean Ser7P at promoters and across gene bodies in all active gene categories (fig. S4 and table S2). We did not examine the effect of Pc depletion on Ser7P. Combined, the above results indicate that Sce or Pc depletion causes global hypophosphorylation of Pol II at active gene promoters, with varying effects in gene bodies, and some significant increases at PcG domain genes.

Ph depletion has more mild and opposite effects on Pol II phosphorylation compared to those caused by Sce and Pc depletion. Metagene analysis reveals that the Ser5P-to-Rpb3 ratio increases at the promoters

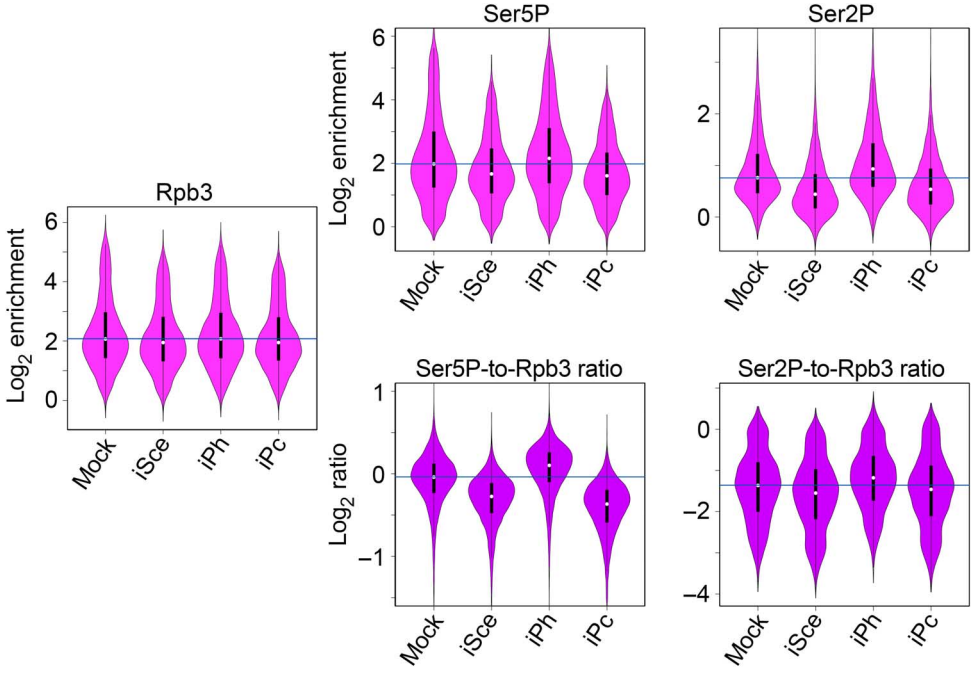

Fig. 5. PRC1 globally alters phosphorylation of Rpb1 heptad repeats at active gene promoters. The violin plots in the left panel show the distribution of total Pol II (Rpb3) occupancy at 7398 active promoters determined from ChIP-seq data (described in Figs. 3 and 4) in mock control, Sce-depleted (iSce), Ph-depleted (iPh), and Pc-depleted (iPc) cells. The blue line indicates the median enrichment level in mock control cells. The top panels show the same for the Ser5P and Ser2P modifications. The same data are illustrated by dot plots in fig. S5. The bottom panels show the ratios of Ser5P and Ser2P to Rpb3 in mock control, Sce-depleted, Ph-depleted, and Pc-depleted cells.

of Ph+ H3K27me3− genes (Fig. 4B and fig. S4). A similar increase is also detected by analysis of all active promoters, as shown by the violin plots in Fig. 5 and dot plots in fig. S5. These modest increases are statistically significant (table S2). The Ser2P and Ser7P levels relative to Rpb3 are also elevated at active promoters by Ph depletion but are similar to the control ratios in gene bodies (Figs. 4B and 5, fig. S4, and table S2). Thus, Ph depletion causes hyperphosphorylation of Pol II at promoters, with a smaller impact in gene bodies.

Our laboratory previously reported that Ph depletion in BG3 cells reduced the Ser2P-to-Rpb3 ratio at active genes (*14*). This study used a polyclonal Ser2P antibody (Abcam #2059). However, a second lot of the same catalog number from the same provider did not give the same results, although both lots show reduced signal in Western blots after treatment of cells with the flavopiridol Cdk9 inhibitor. We posit that the Abcam antibody recognition of Rpb1 is Ser2P-dependent, but that additional modifications of the heptad repeat alter antibody specificity, and that the two lots vary in this regard. In contrast, the Ser2P antibody used in the current studies (#13499, Cell Signaling Technology) is a rabbit monoclonal, and its specificity and sensitivity to additional modifications have been carefully demonstrated using differentially modified peptides (https://media.cellsignal.com/pdf/13499.pdf). It specifically recognizes Ser2P and not other modifications, and its recognition of Ser2P is blocked by additional modifications in the heptad.

On the basis of the previous published data, it was postulated that PRC1 prevents premature entry of hypophosphorylated Pol II into elongation (*14*, *17*). Our current results indicate that the situation is more complex. The overall picture that emerges is that whereas Sce and Pc facilitate Pol II phosphorylation at active gene promoters, Ph inhibits phosphorylation. We theorize that these opposing activities may help maintain the appropriate phosphorylation levels and possibly aid transcriptional pausing. For instance, Sce and Pc may assist transcription initiation by promoting Ser^5 phosphorylation, and Ph subsequently inhibits elongation by dampening additional phosphorylation.

Although Sce and Ph depletions have opposing effects on Pol II phosphorylation at active promoters, their effects on Thr^4 phosphorylation (Thr4P) near the ends of genes are similar. Sce depletion reduces the Thr4P-to-Rpb3 ratio at gene ends, and Ph depletion reduces Thr4P slightly throughout gene bodies and at the peak of Thr4P at gene ends (Fig. 4B and fig. S4). These effects are mild but consistent with the apparent differences in transcription processing and/or termination detected by 3′ NT-seq described above.

At first sight, the mild hyperphosphorylation of Pol II at active genes caused by Ph depletion is consistent with the finding that Ph depletion causes more significant and direct increases than decreases in RNA production by active genes (Fig. 1). Hyperphosphorylation might be expected to increase elongation and RNA processing efficiency through increased binding of elongation and processing factors. However, Sce depletion causes Pol II hypophosphorylation but still has similar (but weaker) effects on RNA production as Ph depletion (Fig. 1 and table S1). Thus, the effects of PRC1 on Pol II phosphorylation likely contribute to, but do not fully explain, the observed effects on transcription and RNA production.

PRC1 modifies Spt5 pausing-elongation factor association with Pol II at active genes

The global changes in Pol II phosphorylation at active genes caused by depletion of PRC1 subunits can potentially alter binding of elongation and RNA processing factors to the Rpb1 CTD. Another critical factor for the recruitment of RNA processing and elongation factors is the Spt5 subunit of the DSIF (DRB sensitivity–inducing factor) complex that interacts with Pol II (*30*). The Spt5 CTD cooperates with the Pol II CTD to recruit several factors. Like the Rpb1 CTD, the Spt5 CTD is also phosphorylated by P-TEFb (positive transcription elongation factor b) to induce transition from pausing to elongation, and phosphorylation is important for the recruitment of other proteins. We thus performed ChIP-seq for Spt5 to test whether PRC1 influences Spt5 association with active genes and Pol II. A typical pattern for Spt5 shows a peak at the promoter and lower enrichment across the gene body, ending near the termination site (Fig. 4A).

Sce depletion (iSce; red) significantly reduces Spt5 levels at promoters of active genes (Fig. 6, A and B, fig. S5, and table S2). There is no significant change at PcG domain genes with Sce depletion (table S2). Ph depletion (iPh; green) slightly decreases Spt5 at promoters of active genes with high levels of Ph (Ph+ H3K27me3−) and at promoters with low Ph (Ph− H3K27me3−). Both changes are statistically significant (table S2). At both gene classes, Ph depletion increases the Spt5-to-Rpb3 ratio in gene bodies, where Sce depletion has little or no effect (Fig. 6A). Ph depletion significantly increases Spt5 levels at PcG domain genes (table S2). Decreases in total Spt5 and the Spt5-to-Rpb3 ratio upon Sce depletion are observed in the violin and dot plots for all active promoters, whereas Ph depletion has a small but significant effect (Fig. 6B, fig. S5, and table S2). Thus, Sce depletion decreases the levels of Spt5 at most active promoters but has little effect on the Spt5 that travels with elongating Pol II into gene bodies, whereas Ph depletion has modest effects on Spt5 at promoters but increases the amount associated with elongating Pol II.

The complex changes in Spt5 levels at active genes upon PRC1 subunit depletion can potentially alter both elongation and RNA processing. Spt5 is an elongation factor that recruits RNA processing proteins, and thus, the increased Spt5-to-Rpb3 ratio in gene bodies upon Ph depletion could contribute to increased RNA production. Spt5 also acts as a pausing factor, and thus, the decrease in Spt5 at promoters upon Sce depletion could increase the transition of paused Pol II into elongation, leading to increased transcription. However, we cannot currently assay the phosphorylation state of Spt5, which is important for its roles as both a pausing and elongation factor, and thus cannot fully evaluate the functional significance of the observed changes in Spt5 levels.

PRC1 influences Spt5 occupancy and Pol II phosphorylation at transcriptional enhancers and PREs

We unexpectedly detected high enrichment of Spt5 at transcriptional enhancers and PREs. As illustrated by the violin plots in Fig. 7A, Rpb3 levels are highest at active promoters, followed by gene bodies and gene ends, with lower but significant levels at enhancers and PREs. As expected, Spt5 levels follow the Rpb3 pattern at active genes, with highest levels at promoters and lower levels in gene bodies. However, the Spt5 levels at enhancers and PREs are greater than in gene bodies. Consequently, the Spt5-to-Rpb3 ratios at enhancers and PREs are substantially higher than in gene bodies (Fig. 7A).

Depletion of Sce or Ph significantly reduces the Spt5 levels at enhancers and PREs and the Spt5-to-Rpb3 ratios (Fig. 7B, fig. S6, and table S2). We restricted this analysis to extragenic enhancers and extragenic PREs, which do not overlap transcription start sites and do not fall within the transcribed regions, so that increased transcription will not influence the results. Although the decrease in absolute Spt5 levels is more apparent with Sce than with Ph depletion, they have opposite effects on Rpb3 levels so that the final Spt5-to-Rpb3 ratios are very similar. Sce depletion also decreased the Ser5P levels at enhancers and PREs (Fig. 7B, fig. S6, and

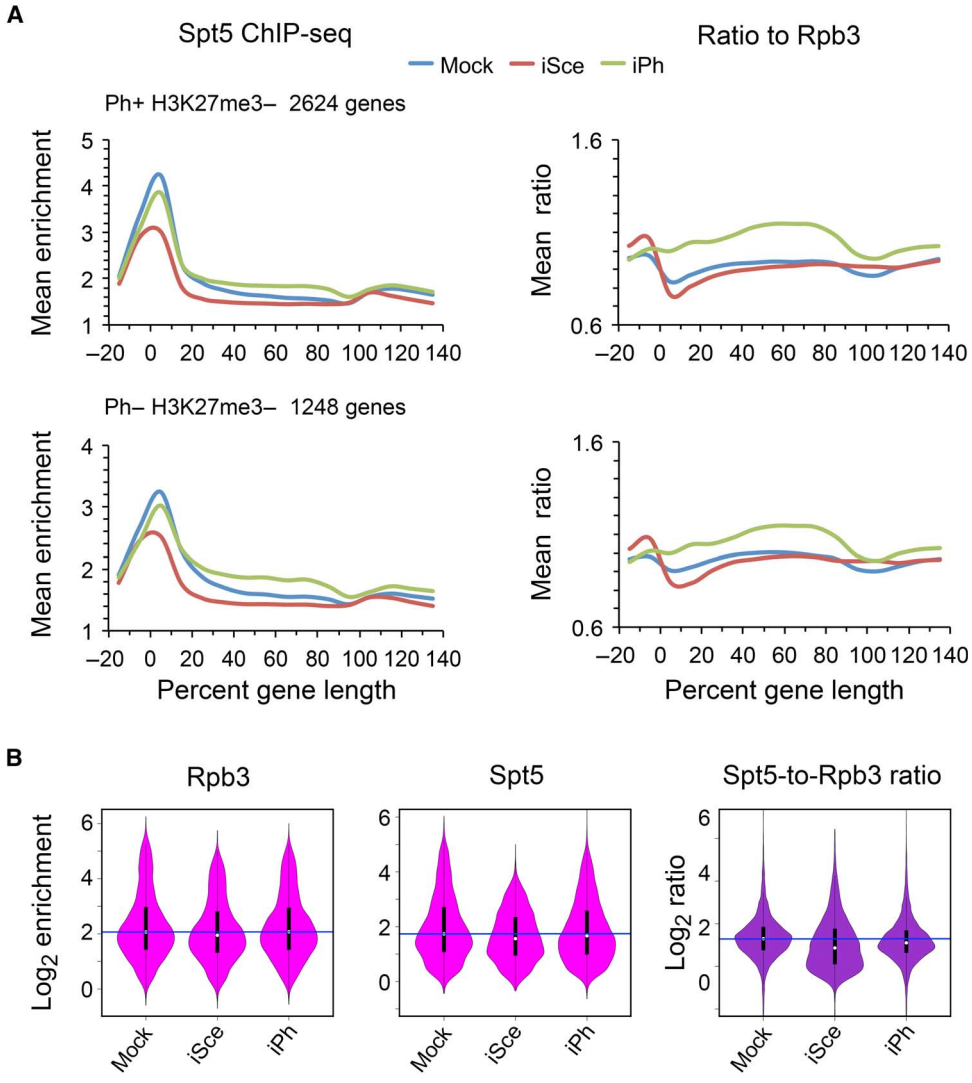

Fig. 6. PRC1 influences the association of the Spt5 pausing-elongation factor with active genes and promoters. (**A**) Metagene analysis of Spt5 ChIP-seq enrichment for Ph+ H3K27me3− and Ph− H3K27me3− active genes in mock control (blue lines), Sce-depleted (iSce; red lines), and Ph-depleted (iPh; green lines) cells. Left: Mean enrichment. Right: Ratio of Spt5 to Rpb3 across the genes. The *P* values from Wilcoxon signed-rank tests are provided in table S2. (**B**) Occupancy of 7398 active promoters by Rpb3 and Spt5 in mock control, Sce-depleted, and Ph-depleted cells, shown in violin plot distributions. Blue lines indicate median values in mock control cells. Dot plots in fig. S5 illustrate the same results. Right: Distribution of the Spt5-to-Rpb3 ratio across all promoters.

table S2), giving rise to little net change in the Ser5P-to-Rpb3 ratio. In contrast, Ph depletion strongly increased Ser5P levels at extragenic PREs, with a significant increase in the Ser5P-to-Rpb3 ratio (Fig. 7B, fig. S6, and table S2). Thus, Ph depletion increases total Pol II levels at PREs, and a significant fraction of this Pol II appears to initiate transcription. On the basis of these findings, we posit that PRC1 suppresses the transcription of enhancers and PREs, preventing them from acting as cryptic promoters.

Sister chromatid cohesion proteins control global PRC1 chromosome–binding dynamics in vivo

The above experiments examining the roles of PRC1 in transcription of active genes were motivated by previous genomic ChIP experiments, indicating that cohesin recruits and sequesters a large fraction of the PRC1 complex at active genes in cultured cells (*14*). The broad influence of PRC1 on active gene transcription, Pol II phosphorylation, and Spt5 levels in cultured cells described above emphasizes the importance of determining whether or not cohesin also modifies PRC1 chromosome binding in vivo. Although PRC1 was detected at active genes in developing tissue by genomic ChIP, the inability to obtain tissue without cohesin prevented the use of ChIP-seq to confirm that cohesin also establishes PRC1 association with active genes in vivo. We thus tested this idea by FRAP (fluorescence recovery after photobleaching) in third-instar larval salivary glands from wild-type and cohesin mutant flies using a transgene that expresses a functional Pc-EGFP (enhanced green fluorescent protein) protein (*31*). Our laboratory previously used FRAP to quantify global cohesin chromosome-binding dynamics in various heterozygous mutant backgrounds (*20*, *32*), indicating that this technique may be sensitive enough to detect a change in Pc chromosome binding in heterozygous cohesin mutants.

We measured global Pc chromosome–binding dynamics by photobleaching half of the nucleus and following the difference in fluorescence (ΔF) between the unbleached and bleached halves over time. The fraction

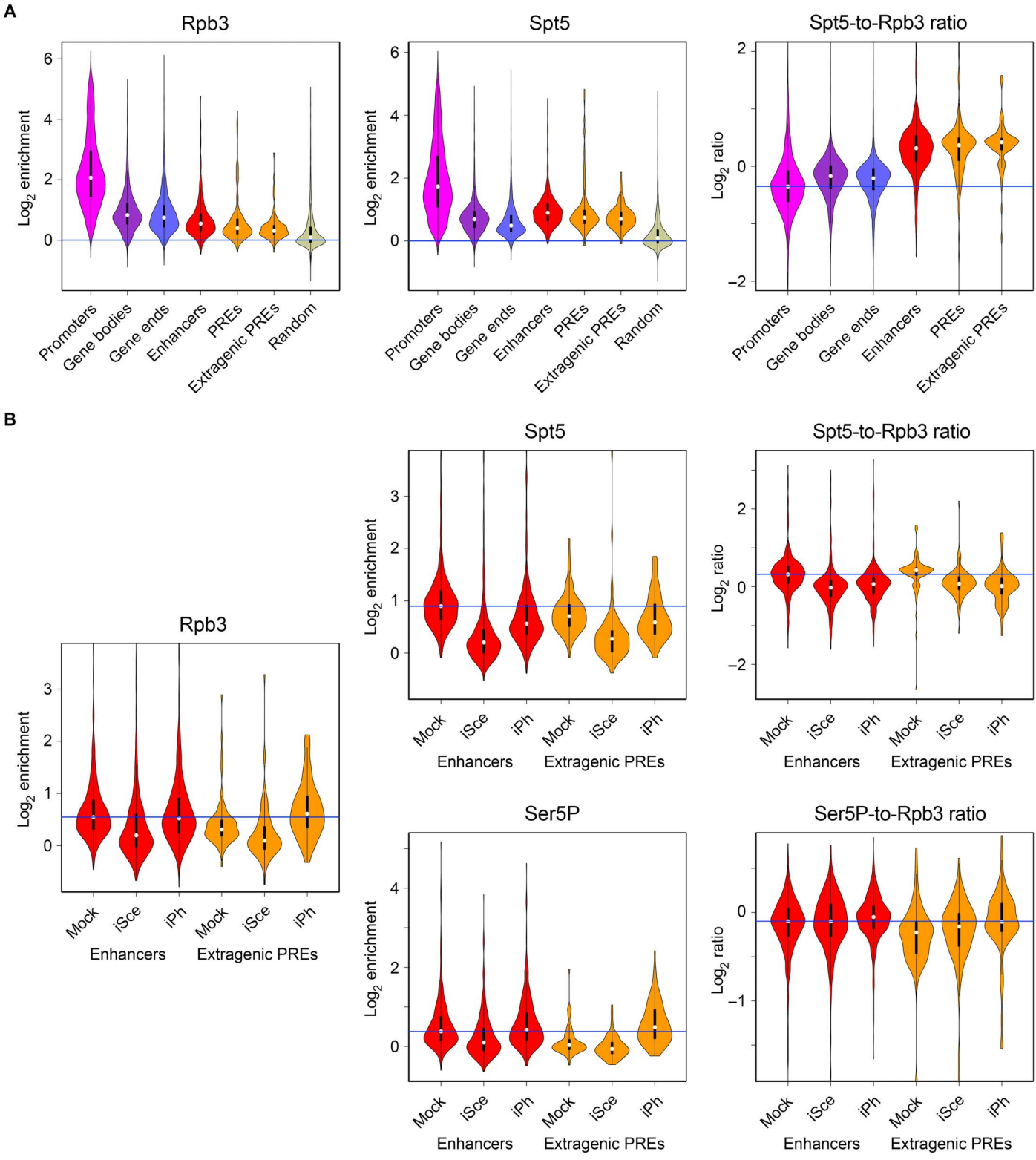

Fig. 7. PRC1 facilitates association of Spt5 and Pol II with enhancers and PREs and influences Pol II phosphorylation. (**A**) Distribution of Rpb3 and Spt5 density across genes and regulatory sequences. The left two panels show the occupancy of Rpb3 and Spt5 at promoters (pink violin distributions), in gene bodies (purple), at gene ends (blue), at extragenic enhancers (red), at PREs and extragenic PREs (orange), and at random sites (tan). The right panel shows the distributions of the Spt5-to-Rpb3 ratio at the same elements. (**B**) Effects of Sce and Ph depletion on Spt5 and Ser5P levels at enhancers and extragenic PREs. The left panel shows the distribution of Rpb3 at extragenic enhancers (red) and PREs (orange) in mock control, Sce-depleted (iSce), and Ph-depleted (iPh) cells. The top left panel shows the same for Spt5, and the bottom left panel shows the same for Ser5P. Dot plots in fig. S6 show the same data. The two right panels show the ratios of Spt5 to Rpb3 (top) and Ser5P to Rpb3 (bottom).

of unbound freely diffusing molecules was estimated by the rapid decrease in fluorescence in the unbleached half of the nucleus that occurs during the short bleaching time, and the recovery curves (Fig. 8A) were fit to multicomponent exponential decay equations to detect Pc-EGFP fractions that bind the chromosomes. The unbound freely diffusing fraction represents nearly half of the total Pc-EGFP, and we distinguished two different chromosome-binding modes by recovery curve analysis. A rapidly equilibrating (fast) fraction of Pc-EGFP with a chromosomal half-life close to 25 s is nearly a third of the total, and close to 20% of Pc-EGFP has a slow chromosomal half-life of 370 ± 49 s (~6 min) (Fig. 8A). Previous Pc-EGFP FRAP studies with individual salivary chromosome bands revealed that Pc-EGFP chromosomal residence times vary from 1 to 10 min depending on the specific location (*33*). Our experiments measured the global Pc-EGFP residence time, and we posit that the 6-min half-life we observe is the average for PRC1 bound to both active and silenced genes.

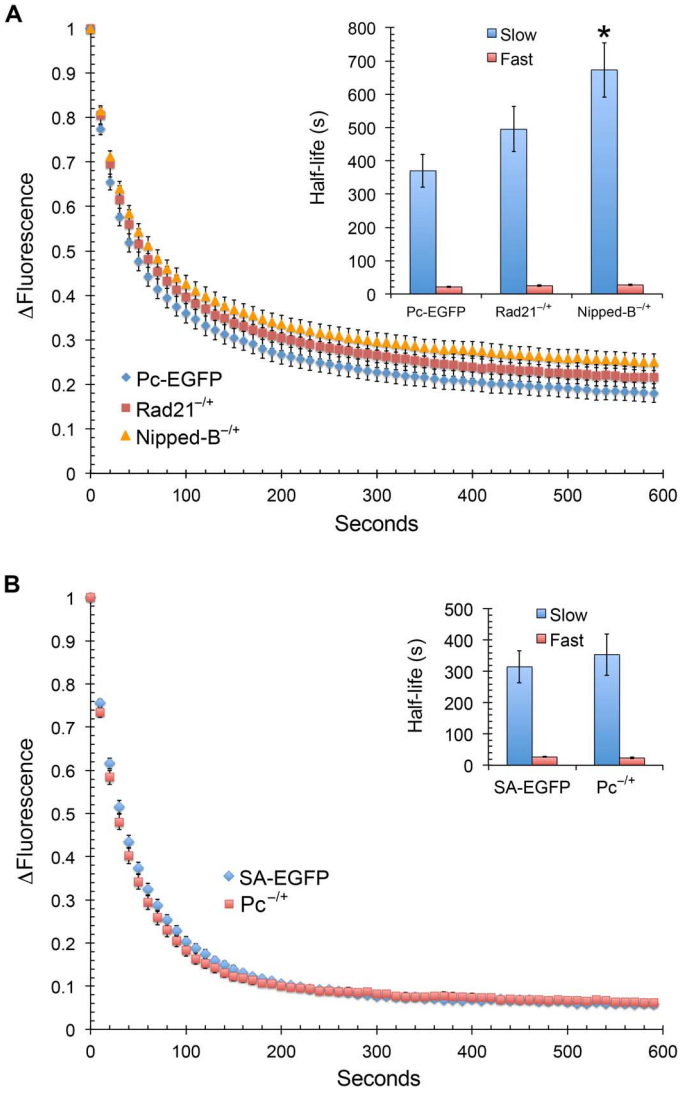

Fig. 8. Nipped-B and cohesin control global Pc chromosome–binding dynamics in vivo. (**A**) FRAP recovery curves for Pc-EGFP in wild-type (blue diamonds), heterozygous *Rad21* (*verthandi*) mutant (*vtd*^{ex15}, Rad21$^{-/+}$, red boxes), and heterozygous *Nipped-B* mutant (*Nipped-B*$^{407/+}$, Nipped-B$^{-/+}$, orange triangles) third-instar larval salivary gland nuclei. At least 30 nuclei were averaged for each curve. Error bars are the SD of the mean. The inset shows the half-lives calculated from the recovery curves for the stable (slow; blue) and less stable (fast; red) binding forms of Pc. Error bars are SDs. The asterisk indicates a statistically significant difference from the control. (**B**) FRAP recovery curves for the SA-EGFP–labeled cohesin subunit in wild-type (SA-EGFP; blue diamonds) and heterozygous *Pc* mutant (*Pc*$^{4/+}$, Pc$^{-/+}$, red boxes) salivary glands. At least 30 nuclei were averaged for each curve, error bars are SDs of the mean, and the inset shows the chromosomal half-lives calculated for the stable (slow; blue) and less stable (fast; red) binding from the recovery curves.

In heterozygous *vtd*^{ex15} (Rad21$^{-/+}$) mutants, the short half-life (fast) is not measurably altered, but the slow half-life increases to 495 ± 68 s (8.25 min) (Fig. 8A). In heterozygous *Nipped-B*^{407} (Nipped-B$^{-/+}$) mutant glands, the half-life of the slow Pc-EGFP fraction increases to 673 ± 82 s (11.2 min) without a change in the fast fraction. This 1.8-fold increase in chromosomal residence time is statistically significant (P = 0.0046, t test), although the smaller 1.3-fold increase in the heterozygous *Rad21* cohesin mutant is not (P = 0.15). These findings demonstrate that reduction of Nipped-B levels globally alters Pc chromosome–binding dynamics. By genomic ChIP, our laboratory previously observed that cohesin depletion reduces Pc levels at active genes and increases Pc levels at PcG-silenced genes (*14*). Therefore, the increase in average chromosomal residence time from 6 min in wild-type glands to 8 and 11 min in cohesin and *Nipped-B* mutant glands suggests that PRC1 binding to silenced genes is more stable than at active genes.

In the previous genomic ChIP experiments in cultured cells, there was no consistent global effect of PRC1 depletion on cohesin levels at active genes beyond increased cohesin at those silenced genes that become active (*14*). Consistent with this observation, we find that a heterozygous *Pc* mutation has no significant effect on the global chromosome-binding dynamics of the SA (stromalin)–EGFP–tagged cohesin subunit in salivary glands, with a slow half-life of 315 ± 51 s in wild-type glands and 354 ± 66 s in heterozygous *Pc*^{4} mutant (Pc$^{-/+}$) glands (Fig. 1B). Combined, the Pc-EGFP and SA-EGFP FRAP experiments support the genomic ChIP experiments in cultured cells and substantiate the idea that cohesin sequesters a significant fraction of PRC1 at active genes in vivo. Thus, it appears that PRC1 is likely to have in vivo effects on active gene transcription similar to those in cultured cells described above.

DISCUSSION

The above findings demonstrate that PRC1 recruited to active genes by the cohesin complex modifies the transcription of active genes. Transcription of several active genes is significantly altered by the depletion of PRC1 subunits, and the significantly affected genes are enriched for those binding higher levels of PRC1. PRC1 subunits broadly influence Pol II phosphorylation (Fig. 9), transcription, and possibly RNA processing near the ends of active genes. PRC1 also widely influences the association of the Spt5 pausing-elongation factor with active genes (Fig. 9), transcriptional enhancers, and PREs.

It is not currently feasible to exhaustively examine all the potential effects of PRC1 on active gene transcription, in part, because of limitations in the knowledge of the mechanisms that control transcription. Although the studies described here explore whether or not PRC1 might affect transcription through effects on Pol II phosphorylation and binding of the Spt5 pausing-elongation factor (Fig. 9), they do not definitively define mechanisms by which PRC1 mediates these effects. However, they establish that PRC1 affects transcription, Pol II modification, and Spt5 levels at most active genes, greatly expanding its potential roles in developmental gene regulation beyond its canonical roles in epigenetic silencing.

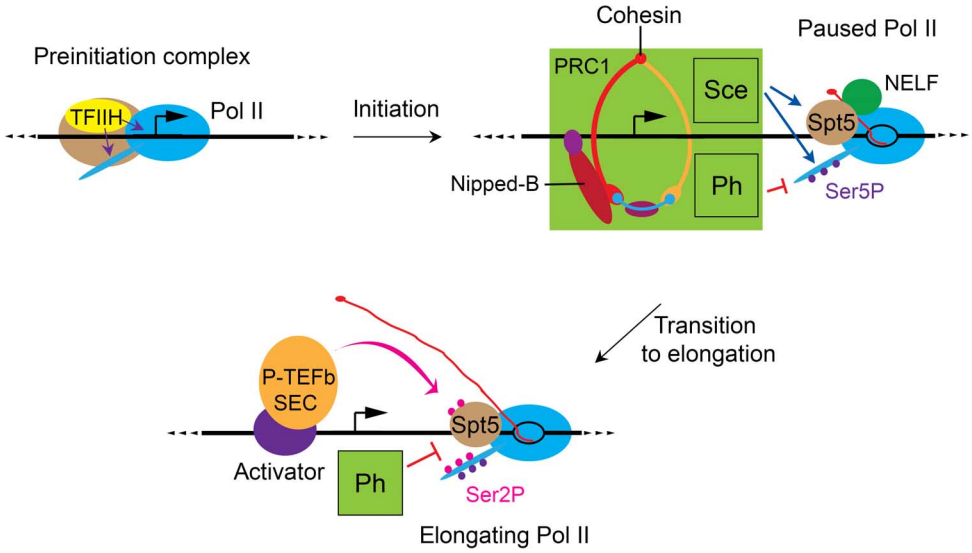

Fig. 9. PRC1 influences Pol II modifications and Spt5 occupancy at active genes. TFIIH in the preinitiation complex (upper left) facilitates DNA unwinding to form the transcription bubble and phosphorylates Ser^5 residues (Ser5P) in the heptad repeats in the CTD of the Rpb1 subunit of Pol II. Binding of Spt5 and NELF (negative elongation factor) pausing factors causes promoter-proximal pausing (upper right). The cohesin complex recruits PRC1 (green box), and the Sce subunit of PRC1 facilitates Ser^5 phosphorylation and Spt5 binding by undefined mechanisms. Ph suppresses Ser5P at the promoter. P-TEFb in the SEC (super elongation complex) recruited by activator proteins phosphorylates Ser^2 residues in the Pol II heptad repeats and Spt5 to start transcription elongation (bottom). Ph suppresses Spt5 association with elongating Pol II. The effects of PRC1 on Pol II and Spt5 coincide with changes, largely increases, in transcription of active genes.

We expect that the impact of PRC1 on active gene transcription would be more marked in developing tissues that completely lack one or more PRC1 subunits than the effects in cultured cells observed here, which occur at many genes with incomplete depletion of PRC1 subunits over a period of a few days. Because PRC1 subunit mutations are homozygous lethal, and development over multiple cell generations will likely have even more indirect effects than the short-term depletion studies presented here, it will be challenging to demonstrate the developmental roles of PRC1 regulation of active genes. This will likely require new and more sensitive technologies for examining transcription and protein binding in small mutant clones of cells. Although our laboratory originally detected PRC1 occupancy of active genes in developing wing tissue (*14*), the presence of multiple cell types and the inability to obtain sufficient pure tissue lacking PRC1 subunits led us to pursue studies in more homogenous cultured cells.

Although consistent with multiple roles for PRC1 in active gene transcription, the effects of PRC1 on Pol II phosphorylation and Spt5 binding described here do not fully explain the observed changes in RNA production. Sce depletion has more modest effects than Ph depletion on transcription, as measured by 3′ NT-seq. Sce, Pc, and Ph depletions all have similar effects on total RNA accumulation, although the effects of Sce depletion are generally weaker. However, these more mild effects are discordant with Sce's stronger effects on the levels of other PRC1 subunits, Pol II phosphorylation, and Spt5 occupancy at active genes. The hypophosphorylation of Pol II caused by Sce depletion is very similar to that caused by Pc depletion and is more marked than the hyperphosphorylation caused by Ph depletion. The decrease in Spt5 caused by Sce depletion at promoters is also more marked. Nonetheless, the apparent changes in transcription density caused by Sce and Ph depletion near the ends of active genes are similar. Therefore, we posit that other unknown actions of PRC1 at active genes are likely to be the more proximate cause of the observed effects on transcription. These might include changes in the interaction of Pol II with other elongation factors such as the Paf1 complex, histone-modifying enzymes, or RNA processing factors, all of which will require extensive new efforts to investigate.

One potential explanation for the differences in the effects of Sce and Ph on transcription and Pol II modifications is that Sce is also a subunit of the dRAF (dRING-associated factors) noncanonical PcG complex, which also contains Psc and the Kdm2 histone demethylase (*34*). Given the similar but weaker effects of Sce depletion than Pc and Ph depletion on total RNA levels, and the similar effects of Sce and Pc depletion on Pol II phosphorylation, it seems unlikely that most global effects of Sce depletion at active genes reflect changes in dRAF activity. However, it is possible that the effects on dRAF function might be involved in a few cases where the effects of Sce depletion differ from those of Pc and Ph.

Once the proximal causes of the effects of PRC1 on transcription are identified, this could open the door to mechanistic studies to determine how PRC1 mediates these changes. Although we know that PRC1 directly interacts with the cohesin complex, it is likely that it also interacts directly and perhaps modifies other proteins that participate in transcription such as Pol II, Pol II kinases, elongation factors, and RNA processing proteins. Consistent with this idea, Ser5P Pol II coimmunoprecipitates with the Pc subunit of PRC1 from cell extracts, and Pc interacts directly with the CREB-binding protein (CBP) acetyltransferase transcriptional coactivator that acetylates histones and other proteins. (*35*). Given that Sce, Pc, and Ph have different effects on Pol II modifications, it is possible that each interacts with different components of the transcriptional machinery.

Whereas the idea that each PRC1 subunit might have a different role in transcriptional control is not surprising, the ability of Pc and Ph to associate with active genes in an independent manner was unexpected. Although ChIP-seq indicates that Ph is more confined to PREs and spreads less across silenced domains than Pc, Ph and Pc occupancies of PREs and silenced regions are co-dependent. In contrast, Pc can be high at active promoters that have lower Ph levels, indicating that the Pc-to-Ph ratio varies between active genes. Moreover, Pc depletion

substantially increases Ph levels at many active promoters. Thus, the different PRC1 subunits not only have different activities but also might act independently of the complete PRC1 complex at active genes.

The unique role of Sce in promoting Pol II phosphorylation and Spt5 binding at promoters, enhancers, and PREs raises the question of the role of the H2Aub modification. Unlike Sce, the H2Aub modification is not required for gene silencing but is essential for viability (*10*). This raises the possibility that H2Aub may play an essential role in transcription of active genes. Our laboratory previously mapped H2Aub genome-wide in BG3 cells and detected only minor levels at most active genes (*36*). However, it is possible that the PR-DUB complex that deubiquitinylates H2A (*37*) is also present and maintains a low steady-state level of this modification.

It remains to be determined how the activities of PRC1 in active gene transcription are related to its functions in gene silencing. The key silencing mechanisms that have been proposed based on in vitro biochemical studies include chromatin compaction, inhibition of nucleosome remodeling, and blocking transcription initiation (*38*–*40*). The finding that Pc inhibits the protein acetylation activity of CBP suggests another mechanism by which PRC1 suppresses transcription (*35*). This latter mechanism is more likely to occur at active genes, given that we do not see evidence for suppression of transcription initiation by PRC1 at active genes. It may be that chromatin conformation mechanisms for repression are stimulated by H3K27me3, which is low at most active genes.

The roles of PRC1 complexes in active gene transcription may be even more complex in mammals, which have multiple alternative subunits that can form many different complexes (*3*, *41*). Association of PRC1 with active genes occurs in differentiating human cells (*13*), and thus, we expect that PRC1 modulation of active gene transcription likely plays significant roles in human development and disease.

MATERIALS AND METHODS

Experimental design

To determine whether PRC1 subunits affect active gene transcription, we performed a number of controlled laboratory experiments: RNA-seq (total RNA), 3′ NT-seq (transcription), and ChIP-seq against multiple forms of RNA Pol II and the Spt5 pausing-elongation factor. These studies were performed using *Drosophila* ML-DmB3-c2 (BG3) cells. Four different BG3 cell treatment groups were used: mock, Ph RNAi, Sce RNAi, and Pc RNAi. To determine whether PRC1 subunits affect active gene expression, at least three independent biological replicates were used for RNA-seq analysis: six mock, three Ph RNAi, three Sce RNAi, and three Pc RNAi. To determine whether PRC1 subunits affect active gene transcription, at least three independent biological replicates were used for 3′ NT-seq: three mock, three Ph RNAi, and four Sce RNAi. To determine whether PRC1 subunits affect the occupancy of RNA Pol II and Spt5, each ChIP-seq experiment was carried out using at least two biological replicates. The ChIP-seq replicates are detailed in table S4. The genome-wide correlation coefficients between normalized replicates were calculated, and the ChIP patterns were examined in a genome browser to ensure reproducibility before averaging the replicates for quantitative analysis.

To determine whether cohesin established PRC1 association with active genes in vivo, controlled laboratory FRAP experiments were carried out using *Drosophila* third-instar larval salivary gland nuclei from wild-type and cohesin mutant flies expressing a Pc-EGFP protein. At least 30 nuclei from each group were measured and averaged for analysis.

BG3 cell culture and RNAi

Drosophila ML-DmBG3-c2 (BG3) cells derived from larval central nervous system were cultured, and proteins were depleted using double-stranded RNA (dsRNA) for 4 to 5 days, as previously described (*42*). The primers used to generate the Ph and Pc dsRNA templates are described elsewhere (*14*, *22*, *36*, *42*). Sce was depleted using two dsRNAs. The primers to make the templates for Sce dsRNA were set A (TAATACGACTCACTATAGGGAGACGACACAGCCTCCAATGATA and TAATACGACTCACTATAGGGAGATGTAGCGCACACAGTTCTCC) and set B (TAATACGACTCACTATAGGGAGATTGAACAACCAAAGTGCGG and TAATACGACTCACTATAGGGAGATGGGACACATCAGTTCGCT). Whole-cell protein extracts were made in lysis buffer [8 M urea, 1% (v/v) NP-40, and 40 mM tris-HCl (pH 7.4)] and analyzed by Western blotting to confirm protein knockdowns. Total RNA was evaluated for the expected derepression of *Abd-B* following knockdown of Ph, Pc, or Sce. Total RNA was isolated using Zymo Quick-RNA MiniPrep Columns (Zymo Research) and assessed by real-time polymerase chain reaction (PCR), as described previously (*42*).

RNA sequencing

Multiple independent biological replicates were performed for all RNA-seq experiments. Total RNA from mock- and RNAi-treated BG3 cells was isolated using Zymo Quick-RNA MiniPrep Columns (Zymo Research) and assessed for quality using an Agilent Bioanalyzer. Total RNA was depleted for ribosomal RNA (rRNA) using the RiboMinus Eukaryote System v2 (Life Technologies), supplementing the kit-provided rRNA probes with an equimolar concentration of custom *Drosophila*-specific rRNA probes (table S3). Sequencing libraries were prepared using the Ion Total RNA-Seq Kit v2 (Life Technologies) and sequenced on an Ion Proton System. RNA coverage of exons was quantified and normalized as previously described (*43*). The expression values in table S1 are the mean normalized nucleotide sequence coverage for each gene.

3′ Nascent RNA-seq

Multiple independent biological replicates were performed for all 3′ NT-seq experiments. Approximately 2×10^8 cells were harvested by centrifugation for 5 min at 1000*g* at 4°C. Chromatin was prepared for nascent RNA isolation, as described elsewhere (*23*). The chromatin pellet was dissolved in 10 ml of TRIzol (Invitrogen), and RNA was isolated following the manufacturer's protocol and precipitated by isopropanol with 0.2 M NaCl and 20 μg of glycogen. Nascent RNA (10 μg) was digested with DNase I (#D9905K, Epicentre) in a total volume of 100 μl for 20 min at 37°C, as described by the manufacturer, except that the reaction included 40 U of SUPERase In RNase Inhibitor (Invitrogen). The digested RNA was diluted to a total volume of 300 μl and extracted with an equal volume of acid phenol–chloroform (Sigma-Aldrich) and precipitated as above. Nascent RNA quality was assessed using an Agilent Bioanalyzer RNA Pico Chip.

Uncapped RNAs in the DNase I–treated nascent RNA were degraded in a two-step reaction to remove rRNA. Nascent RNA (4 μg) was treated with RNA 5′ polyphosphatase (#RP8092H, Epicentre) in a total reaction volume of 20 μl (including 20 U of SUPERase In) at 37°C for 30 min to convert 5′-triphosphates to monophosphates. The treated RNA was diluted with water to a total volume of 200 μl and purified using the Ion Torrent RNA-Seq Magnetic Bead Cleanup Module (Life Technologies). The diluted RNA was added to 10 μl of magnetic nucleic acid–binding beads, 268 μl of binding solution concentrate, and 668 μl of ethanol. After washing the beads as recommended by the manufacturer, the RNA was

eluted in 16 µl of H_2O at 70°C. RNAs were treated with Terminator 5′-Phosphate-Dependent Exonuclease (#TER51020, Epicentre) in a total reaction volume of 20 µl (including 20 U of SUPERase In) at 30°C for 60 min to degrade RNAs with 5′-monophosphates. The treated RNA was diluted with water to a total volume of 100 µl and purified by binding to 5 µl of nucleic acid–binding beads in 134 µl of binding solution concentrate and 334 µl of ethanol. The RNA was eluted in 10 µl of H_2O at 70°C.

To remove residual contaminating mRNAs, the cap-selected nascent RNA was subjected to three sequential poly(A) RNA depletions using oligo d(T) dynabeads (Ambion) following the manufacturer's protocol, keeping RNA that does not bind to the oligo d(T) beads. Five microliters of oligo d(T) dynabeads was washed with 2× binding buffer [20 mM tris-HCl (pH 7.5), 1 M LiCl, and 2 mM EDTA] twice and suspended in 9 µl of 2× binding buffer plus 1 µl (20 U) of SUPERase In. The RNA was denatured at 65°C for 2 min and incubated for 5 min at room temperature with oligo d(T) dynabeads in a total volume of 20 µl. The supernatant was collected, and the poly(A) depletion was repeated two more times. The poly(A)-depleted nascent RNA in the final supernatant was diluted to a total volume of 100 µl with H_2O and bound to 5 µl of magnetic nucleic acid–binding beads in 134 µl of binding solution concentrate and 334 µl of ethanol. After washing the beads, RNA was eluted with 12 µl of H_2O at 70°C. The expected yield was 15 to 20% of the 4 µg of input RNA. RNA quality was assessed using an Agilent Bioanalyzer RNA Pico Chip.

Sequencing libraries were made from the final nascent RNA using reagents in the Ion Total RNA-Seq Kit v2 (Life Technologies) with a modified protocol to capture the native 3′ ends of RNA transcripts. The modified protocol requires separate 5′ and 3′ adapters, which are not provided in the kit but were obtained from the manufacturer (Life Technologies). Following the manufacturer's protocol for adapter ligation, 100 ng of nascent RNA was ligated to 0.5 µl of 3′ adaptor in a total reaction volume of 10 µl. The ligation reaction was diluted to a total volume of 100 µl, and the 3′ adapter–ligated RNA was bound to 5 µl of magnetic nucleic acid–binding beads in 134 µl of binding solution concentrate and 334 µl of ethanol. The RNA was eluted in 10 µl of H_2O at 70°C. The eluted RNA was digested with ribonuclease III in a total volume of 12 µl for 4 min at 37°C and immediately diluted with 18 µl of ice-cold water. The fragmented RNA was bound to 5 µl of magnetic nucleic acid–binding beads in 90 µl of binding solution concentrate and 150 µl of ethanol. RNA was eluted with 12 µl of H_2O at 37°C, and the volume was reduced to 2 µl using a speed-vac. 5′ Adapter ligation was performed as described above for the 3′ adapter. Following 5′ adapter ligation, reverse transcription and PCR amplification were conducted as per the manufacturer's protocol. Libraries were sequenced on an Ion Torrent Proton System.

The 3′ NT-seq fastq files were aligned in two steps. They were first aligned to a fasta file containing the *Drosophila melanogaster* release 5.9 pre-rRNA, ncRNA (noncoding RNA), and miscRNA (miscellaneous RNA) sequences using the TMAP (Torrent Mapping Program) aligner (*44*), allowing both 5′ and 3′ clipping and setting a minimum seed length of 20. The reads that did not align were selected using SAMtools (*45*) and aligned to the *D. melanogaster* (April 2006) genome sequence without allowing clipping. The aligned reads were sorted and indexed using SAMtools, and BEDTools (*46*) was used to calculate genome coverage. Using a custom R (*47*) script (sum.bed.r; file S1) and strand-specific files, the total gene sequence coverage was calculated and used to normalize coverage across all samples, as previously described, using a whole-gene bed file (file S2). 3′ NT-seq bam files were converted to normalized sgr files using BEDTools and a custom R script and visualized using the Integrated Genome Browser (*48*). For comparison to RNA-seq data, 3′ NT-seq coverage was calculated across the entire annotated genes using the whole-gene bed file (file S2). Analysis of 3′ NT-seq density in exons and introns and upstream and downstream of potential polyadenylation signals was conducted using the sgr files and bed files generated from the positions of all active gene exons greater than 500 nt (file S3) and potential poly(A) signals (file S4). Metagene analysis of 3′ NT-seq data was conducted using an R script (metagene.plus.minus.r; file S1); the normalized sgr files and bed files for the indicated extended gene classes were described in the main text and figure legends (files S5 to S8). The ratios were calculated for each gene individually and then averaged.

ChIP sequencing

Multiple (at least two) independent biological replicates were performed for all ChIP-seq experiments and analyzed using the procedures detailed elsewhere (*25*, *49*). The phosphorylated Pol II rabbit monoclonal antibodies were purchased from Cell Signaling Technology: Ser5P (#13523), Ser2P (#13499), Ser7P (#13780), and Thr4P (#26319). K. Adelman (National Institute of Environmental Health Sciences) provided the Rpb3 antibody. J. Lis (Cornell University) provided the Spt5 antibody. R. Jones (Southern Methodist University) provided the Pc antibody, and J. Müller (Max Planck Institute of Biochemistry) provided the Ph antibody.

To ensure accuracy and reproducibility, all ChIP replicates were sequenced to at least 10× genome coverage and were normalized to input samples sequenced to at least 45× genome coverage. Several samples were normalized to published input samples (*25*), and because of a slight change in the ChIP protocol during the course of these studies that slightly altered the sequence distributions, the rest were normalized to a new input (this study). Table S4 lists the ChIP replicates and the input samples used for normalization. The genome-wide correlation coefficients between normalized replicates were calculated, and the ChIP patterns were examined in a genome browser to ensure reproducibility before averaging the replicates for quantitative analysis. Quantification of ChIP enrichment for gene regulatory sequences, defined as 500-bp elements, was conducted using active promoter, enhancer, and PRE bed files for BG3 cells, as described elsewhere (*25*). Metagene analysis of ChIP-seq enrichment was conducted using a custom R script (metagene.chip.seq.r; file S1) and the indicated extended gene bed files (files S5 to S8). The ratios were calculated for each gene individually and then averaged.

Gene classification

Ph ChIP-seq and modENCODE H3K27me3 ChIP-chip data were used to classify genes. The Integrated Genome Browser was used to generate bed files of regions ≥300 bp in length with Ph and H3K27me3 at the 95th and 99th percentile enrichment. BEDTools was used with the 95th percentile bed files to classify genes as Ph+ H3K27me3+, Ph+ H3K27me3−, and Ph− H3K27me3−. Genes that overlap the 99th percentile bed files for Ph and H3K27me3 were visually inspected in the browser to identify those in which H3K27me3 enrichment at the 99th percentile extended over the entire length of a gene or gene complex. These were defined as PcG domain genes, all of which showed Pc enrichment in the 99th percentile.

Fluorescent recovery after photobleaching

FRAP and data analysis was conducted using salivary glands from control and mutants indicated in the main text, as previously described (*32*). The SA-EGFP cohesin subunit fusion transgene was described elsewhere (*32*). Pc-EGFP fusion transgenic flies were provided by R. Paro (*31*).

Statistical analysis

For RNA-seq and 3′ NT-seq analysis, expressed genes were defined as those that show greater than the median mock total RNA level either in mock control cells or in Ph- or Sce-depleted cells. By this definition, half the annotated genes are expressed in control cells, and those genes that become activated upon Ph or Sce depletion are included. The *t* test was used to calculate *P* values for each expressed gene after Ph, Sce, or Pc depletion. The distribution of *P* values for all genes was used to calculate *q* values for each gene. Significant changes in expression or transcription are those with a *q* value less than or equal to 0.05, equivalent to a 5% false discovery rate. The *P* and *q* values are provided in table S1. Fisher's exact test was used to determine whether genes that significantly change are enriched for those that bind high levels of Ph. The parameters for defining high Ph binding are described in Materials and Methods.

For ChIP-seq analysis, replicates were tested for their genome-wide correlation to ensure reproducibility and then averaged to perform further analysis. For metagene analysis, we used the Wilcoxon signed-rank nonparametric paired test of medians to determine statistically significant changes in the peak bin. The same test was used to determine statistical significance in changes at gene regulatory sequences. The ChIP-seq *P* values are provided in table S2.

SUPPLEMENTARY MATERIALS

Supplementary material for this article is available at http://advances.sciencemag.org/cgi/content/full/3/8/e1700944/DC1

fig. S1. Comparison of effects of Sce, Pc, and Ph depletion on total RNA accumulation in BG3 cells.
fig. S2. Effects of Sce and Pc depletion on Ph occupancy of PREs, active promoters, and extragenic enhancers measured by ChIP-seq.
fig. S3. Effects of Sce and Ph depletion on Pc occupancy of PREs, active promoters, and extragenic enhancers measured by ChIP-seq.
fig. S4. PRC1 modifies Rpb1 phosphorylation at active genes.
fig. S5. Effects of Sce, Ph, and Pc depletion on Rpb3, Ser5P, Ser2P, and Spt5 occupancy of active promoters measured by ChIP-seq.
fig. S6. Effects of Sce and Ph depletion on Rpb3, Ser5P Rpb1, and Spt5 levels at extragenic enhancers and extragenic PREs measured by ChIP-seq.
table S1. RNA-seq quantification and gene ontology.
table S2. Statistical analysis of ChIP-seq data.
table S3. Ribosomal RNA depletion oligonucleotides.
table S4. ChIP-seq replicates and inputs used for normalization.
file S1. R scripts.
file S2. Whole-gene bed file for 3′ NT-seq quantification.
file S3. Active gene exons greater than 500 nt in length.
file S4. Potential active gene poly(A) signals.
file S5. Extended length active gene bed file for genes with high Ph and low H3K27me3 for metagene analysis.
file S6. Extended length active gene bed file for genes with low Ph and low H3K27me3 for metagene analysis.
file S7. Extended length active gene bed file for genes with high Ph and high H3K27me3 for metagene analysis.
file S8. Extended length active gene bed file for PcG domain genes for metagene analysis.

REFERENCES AND NOTES

1. S. Aranda, G. Mas, L. Di Croce, Regulation of gene transcription by Polycomb proteins. *Sci. Adv.* **1**, e1500737 (2015).
2. S. J. Geisler, R. Paro, Trithorax and Polycomb group-dependent regulation: A tale of opposing activities. *Development* **142**, 2876–2887 (2015).
3. A. Piunti, A. Shilatifard, Epigenetic balance of gene expression by Polycomb and COMPASS families. *Science* **352**, aad9780 (2016).
4. Y. B. Schwartz, V. Pirrotta, A new world of Polycombs: Unexpected partnerships and emerging functions. *Nat. Rev. Genet.* **14**, 853–864 (2013).
5. J.A. Simon, R. E. Kingston, Occupying chromatin: Polycomb mechanisms for getting to genomic targets, stopping transcriptional traffic, and staying put. *Mol. Cell* **49**, 808–824 (2013).
6. P. A. Steffen, L. Ringrose, What are memories made of? How Polycomb and Trithorax proteins mediate epigenetic memory. *Nat. Rev. Mol. Cell Biol.* **15**, 340–356 (2014).
7. A. R. Pengelly, Ö. Copur, H. Jäckle, A. Herzig, J. Müller, A histone mutant reproduces the phenotype caused by loss of histone-modifying factor Polycomb. *Science* **339**, 698–699 (2013).
8. R. Cao, L. Wang, H. Wang, L. Xia, H. Erdjument-Bromage, P. Tempst, R. S. Jones, Y. Zhang, Role of histone H3 lysine 27 methylation in Polycomb-group silencing. *Science* **298**, 1039–1043 (2002).
9. H. Wang, L. Wang, H. Erdjument-Bromage, M. Vidal, P. Tempst, R. S. Jones, Y. Zhang, Role of histone H2A ubiquitination in Polycomb silencing. *Nature* **431**, 873–878 (2004).
10. A. R. Pengelly, R. Kalb, K. Finkl, J. Müller, Transcriptional repression by PRC1 in the absence of H2A monoubiquitylation. *Genes Dev.* **29**, 1487–1492 (2015).
11. A. Frangini, M. Sjöberg, M. Roman-Trufero, G. Dharmalingam, V. Haberle, T. Bartke, B. Lenhard, M. Malumbres, M. Vidal, N. Dillon, The aurora B kinase and the polycomb protein ring1B combine to regulate active promoters in quiescent lymphocytes. *Mol. Cell* **51**, 647–661 (2013).
12. T. Kondo, K. Isono, K. Kondo, T. A. Endo, S. Itohara, M. Vidal, H. Koseki, *Polycomb* potentiates *Meis2* activation in midbrain by mediating interaction of the promoter with a tissue-specific enhancer. *Dev. Cell* **28**, 94–101 (2014).
13. V. Loubiere, A. Delest, A. Thomas, B. Bonev, B. Schuettengruber, S. Sati, A. M. Martinez, G. Cavalli, Coordinate redeployment of PRC1 proteins suppresses tumor formation during *Drosophila* development. *Nat. Genet.* **48**, 1436–1442 (2016).
14. C. A. Schaaf, Z. Misulovin, M. Gause, A. Koenig, D. W. Gohara, A. Watson, D. Dorsett, Cohesin and Polycomb proteins functionally interact to control transcription at silenced and active genes. *PLOS Genet.* **9**, e1003560 (2013).
15. G. Strübbe, C. Popp, A. Schmidt, A. Pauli, L. Ringrose, C. Beisel, R. Paro, Polycomb purification by in vivo biotinylation tagging reveals cohesin and Trithorax group proteins as interaction partners. *Proc. Natl. Acad. Sci. U.S.A.* **108**, 5572–5577 (2011).
16. D. Dorsett, M. Merkenschlager, Cohesin at active genes: A unifying theme for cohesin and gene expression from model organisms to humans. *Curr. Opin. Cell Biol.* **25**, 327–333 (2013).
17. D. Dorsett, J. A. Kassis, Checks and balances between cohesin and polycomb in gene silencing and transcription. *Curr. Biol.* **24**, R535–R539 (2014).
18. G. Hallson, M. Syrzycka, S. A. Beck, J. A. Kennison, D. Dorsett, S. L. Page, S. M. Hunter, R. Keall, W. D. Warren, H. W. Brock, D. A. R. Sinclair, B. M. Honda, The *Drosophila* cohesin subunit *Rad21* is a *trithorax* group (trxG) protein. *Proc. Natl. Acad. Sci. U.S.A.* **105**, 12405–12410 (2008).
19. J. A. Kennison, J. W. Tamkun, Dosage-dependent modifiers of polycomb and antennapedia mutations in *Drosophila*. *Proc. Natl. Acad. Sci. U.S.A.* **85**, 8136–8140 (1988).
20. M. D. Cunningham, M. Gause, Y. Cheng, A. Noyes, D. Dorsett, J. A. Kennison, J. A. Kassis, Wapl antagonizes cohesin binding and promotes Polycomb-group silencing in *Drosophila*. *Development* **139**, 4172–4179 (2012).
21. A. Fay, Z. Misulovin, J. Li, C. A. Schaaf, M. Gause, D. S. Gilmour, D. Dorsett, Cohesin selectively binds and regulates genes with paused RNA polymerase. *Curr. Biol.* **21**, 1624–1634 (2011).
22. C. A. Schaaf, H. Kwak, A. Koenig, Z. Misulovin, D. W. Gohara, A. Watson, Y. Zhou, J. T. Lis, D. Dorsett, Genome-wide control of RNA polymerase II activity by cohesin. *PLOS Genet.* **9**, e1003382 (2013).
23. C. M. Weber, S. Ramachandran, S. Henikoff, Nucleosomes are context-specific, H2A.Z-modulated barrier to RNA polymerase. *Mol. Cell* **53**, 819–830 (2014).
24. L. S. Churchman, J. S. Weissman, Nascent transcript sequencing visualizes transcription at nucleotide resolution. *Nature* **469**, 368–373 (2011).
25. A. Swain, Z. Misulovin, M. Pherson, M. Gause, K. Mihindukulasuriya, R. A. Rickels, A. Shilatifard, D. Dorsett, Drosophila TDP-43 RNA-binding protein facilitates association of sister chromatid cohesion proteins with genes, enhancers and Polycomb response elements. *PLOS Genet.* **12**, e1006331 (2016).
26. I. Jonkers, H. Kwak, J. T. Lis, Genome-wide dynamics of Pol II elongation and its interplay with promoter proximal pausing, chromatin, and exons. *eLife* **3**, e02407 (2014).
27. J. L. Corden, RNA polymerase II C-terminal domain: Tethering transcription to transcript and template. *Chem. Rev.* **113**, 8423–8455 (2013).
28. M. Sansó, R. P. Fisher, Pause, play, repeat: CDKs push RNAP II's buttons. *Transcription* **4**, 146–152 (2013).
29. K. M. Harlen, K. L. Trotta, E. E. Smith, M. M. Mosaheb, S. M. Fuchs, L. S. Churchman, Comprehensive RNA polymerase II interactomes reveal distinct and varied roles for each phospho-CTD residue. *Cell Rep.* **15**, 2147–2158 (2016).
30. G. A. Hartzog, J. Fu, The Spt4-Spt5 complex: A multi-faceted regulator of transcription elongation. *Biochim. Biophys. Acta* **1829**, 105–115 (2013).
31. S. Dietzel, H. Niemann, B. Brückner, C. Maurange, R. Paro, The nuclear distribution of Polycomb during *Drosophila melanogaster* development shown with a GFP fusion protein. *Chromosoma* **108**, 83–94 (1999).
32. M. Gause, Z. Misulovin, A. Bilyeu, D. Dorsett, Dosage-sensitive regulation of cohesin chromosome binding and dynamics by Nipped-B, Pds5, and Wapl. *Mol. Cell Biol.* **30**, 4940–4951 (2010).

33. G. Ficz, R. Heintzmann, D. J. Arndt-Jovin, Polycomb group protein complexes exchange rapidly in living *Drosophila*. *Development* **132**, 3963–3976 (2005).
34. A. Lagarou, A. Mohd-Sarip, Y. M. Moshkin, G. E. Chalkley, K. Bezstarosti, J. A. A. Demmers, C. P. Verrijzer, dKDM2 couples histone H2A ubiquitylation to histone H3 demethylation during Polycomb group silencing. *Genes Dev.* **22**, 2799–2810 (2008).
35. F. Tie, R. Banergee, C. Fu, C. A. Stratton, M. Fang, P. J. Harte, Polycomb inhibits histone acetylation by CBP by binding directly to its catalytic domain. *Proc. Natl. Acad. Sci. U.S.A.* **113**, E744–E753 (2016).
36. C. A. Schaaf, Z. Misulovin, M. Gause, A. Koenig, D. Dorsett, The Drosophila *Enhancer of split* gene complex: Architecture and coordinate regulation by notch, cohesin, and polycomb group proteins. *G3* **3**, 1785–1794 (2013).
37. J. C. Scheuermann, A. G. de Ayala Alonso, K. Oktaba, N. Ly-Hartig, R. K. McGinty, S. Fraterman, M. Wilm, T. W. Muir, J. Müller, Histone H2A deubiquitinase activity of the Polycomb repressive complex PR-DUB. *Nature* **465**, 243–247 (2010).
38. N. J. Francis, R. E. Kingston, C. L. Woodcock, Chromatin compaction by a polycomb group protein complex. *Science* **306**, 1574–1577 (2004).
39. M. Lavigne, N. J. Francis, I. F. G. King, R. E. Kingston, Propagation of silencing. *Mol. Cell* **13**, 415–425 (2004).
40. L. Lehmann, R. Ferrari, A. A. Vashisht, J. A. Wohlschlegel, S. K. Kurdistani, M. Carey, Polycomb repressive complex 1 (PRC1) disassembles RNA polymerase II preinitiation complexes. *J. Biol. Chem.* **287**, 35784–35794 (2012).
41. K. E. Connelly, E. C. Dykhuizen, Compositional and functional diversity of canonical PRC1 complexes in mammals. *Biochim. Biophys. Acta* **1860**, 233–245 (2017).
42. C. A. Schaaf, Z. Misulovin, G. Sahota, A. M. Siddiqui, Y. B. Schwartz, T. G. Kahn, V. Pirrotta, M. Gause, D. Dorsett, Regulation of the *Drosophila Enhancer of split* and *invected-engrailed* gene complexes by sister chromatid cohesion proteins. *PLOS ONE* **4**, e6202 (2009).
43. Y. Wu, M. Gause, D. Xu, Z. Misulovin, C. A. Schaaf, R. C. Mosarla, E. Mannino, M. Shannon, E. Jones, M. Shi, W.-F. Chen, O. L. Katz, A. Sehgal, T. A. Jongens, I. D. Krantz, D. Dorsett, Drosophila *Nipped-B* mutants model Cornelia de Lange Syndrome in growth and behavior. *PLOS Genet.* **11**, e1005655 (2015).
44. N. Homer, TMAP: The Torrent Mapping Program (2011); https://github.com/iontorrent/TMAP/blob/master/doc/tmap-book.pdf.
45. H. Li, B. Handsaker, A. Wysoker, T. Fennell, J. Ruan, N. Homer, G. Marth, G. Abecasis, R. Durbin; 1000 Genome Project Data Processing Subgroup, The sequence alignment/map format and SAMtools. *Bioinformatics* **25**, 2078–2079 (2009).
46. A. R. Quinlan, I. M. Hall, BEDTools: A flexible suite of utilities for comparing genomic features. *Bioinformatics* **26**, 841–842 (2010).
47. R Core Team, *R: A Language and Environment for Statistical Computing* (R Foundation for Statistical Computing, 2015); www.r-project.org.
48. J. W. Nicol, G. A. Helt, S. G. Blanchard Jr., A. Raja, A. E. Loraine, The Integrated Genome Browser: Free software for distribution and exploration of genome-scale datasets. *Bioinformatics* **25**, 2730–2731 (2009).
49. D. Dorsett, Z. Misulovin, Measuring sister chromatid cohesion protein genome occupancy in *Drosophila melanogaster* by ChIP-seq. *Methods Mol. Biol.* **1515**, 125–139 (2017).

Acknowledgments: We thank C. Weber and S. Henikoff for advice and protocols for nascent RNA-seq and S. Peterson (Life Technologies) for providing Ion Torrent adapters. We also thank K. Adelman, R. Jones, J. Lis, and J. Müller for providing antibodies and R. Paro for the Pc-EGFP transgene. **Funding:** This work was supported by NIH National Institute of General Medical Sciences grant GM108872 to D.D. **Author contributions:** M.P., Z.M., and M.G. conducted experiments. M.P., M.G., K.M., and D.D. performed data analysis. M.P., A.S., and D.D. wrote R scripts for data analysis. M.P. and D.D. wrote the paper. **Competing interests:** The authors declare that they have no competing interests. **Data and materials availability:** All data needed to evaluate the conclusions in the paper are present in the paper and/or the Supplementary Materials. Additional data related to this paper may be requested from the authors. Raw high-throughput sequencing data will be deposited in the National Center for Biotechnology Information GEO public database under accession number GSE100548.

Submitted 25 March 2017
Accepted 28 June 2017
Published 2 August 2017
10.1126/sciadv.1700944

Citation: M. Pherson, Z. Misulovin, M. Gause, K. Mihindukulasuriya, A. Swain, D. Dorsett, Polycomb repressive complex 1 modifies transcription of active genes. *Sci. Adv.* **3**, e1700944 (2017).